
University of Frankfurt am Main

Master Thesis

# Computations at Fixed Topology in the Two Dimensional Lattice Schwinger Model

*Author:*
Christopher Czaban

*Supervisor / 1st examiner:*
Prof. Dr. Marc Wagner
*2nd examiner:*
Prof. Dr. Owe Philipsen

*A thesis submitted in fulfilment of the requirements for the degree of Master of Science*

November 2013

# Declaration of Authorship

I, Christopher Czaban, declare that this thesis titled, 'Computations at Fixed Topology in the Two Dimensional Lattice Schwinger Model' and the work presented in it are my own. I confirm that:

- This work was done wholly or mainly while in candidature for a research degree at this University.
- Where any part of this thesis has previously been submitted for a degree or any other qualification at this University or any other institution, this has been clearly stated.
- Where I have consulted the published work of others, this is always clearly attributed.
- Where I have quoted from the work of others, the source is always given. With the exception of such quotations, this thesis is entirely my own work.
- I have acknowledged all main sources of help.

Signed: _____

Date: _____

# *Abstract*

At small lattice spacing and fermion mass QCD simulations are expected to become stuck in a single topological sector. Observables evaluated in a fixed topological sector differ from their counterparts in full QCD, i.e. at unfixed topology, by volume dependent corrections. These corrections are investigated in the two-flavor Schwinger model, which is in several aspects similar to QCD, using Wilson fermions. The attempt is made to remove these corrections by suitable extrapolations to infinite volume.

# Contents

# Chapter 1

# Introduction

At small values of the lattice spacing QCD simulations on the lattice are expected to suffer from frozen topology independent of the quark discretization. The reason is that gauge link configurations belong to different topological sectors, which are separated by barriers of rather large Euclidean action. Choosing a smaller value for the lattice spacing increases these barriers, until standard Hybrid Monte Carlo (HMC) simulation algorithms are not anymore able to frequently tunnel through these barriers. Then a simulation can get stuck in a certain topological sector for a long period of time. In this case computed observables are plagued by corresponding systematic errors (cf. e.g. [1] and references therein). When using overlap fermions topology freezing is even observed at rather coarse lattice spacings [2]. A possible solution to these problems is to restrict computations to a single topological sector, either by sorting the generated gauge link configurations with respect to their topological charge or by directly employing so-called topology fixing actions (cf. e.g. [3–5]). In a second step systematic effects due to topology fixing need to be removed by suitable extrapolations. Corresponding expressions have been derived [6, 7] and tested in simple models, i.e. in the Schwinger model [8] and in quantum mechanics [9].

In this work computations are performed in fixed topological sectors in the Schwinger model with Wilson fermions. In contrast to e.g. overlap fermions, they are computationally much cheaper and therefore allow to generate lattice results for many different topological sectors and spacetime volumes. In addition to the pseudoscalar meson mass the static $q\bar{q}$ potential is also studied.

This work is divided into 5 chapters and one appendix chapter. The main part of this work starts in the second chapter which contains the theoretical foundations. At first the most important points concerning the Schwinger model which are relevant for the investigations are pointed out. Afterwards the theoretical concept of the topological charge in the continuum, as well as on the lattice is explained which is one of the basic principles the computations are based on. In the last section of the theoretical foundations a method will be presented which allows to remove the aforementioned systematic effects by extrapolations. Chapter three contains a concise presentation of the Hybrid Monte Carlo (HMC) algorithm used for this work, including the implemented optimization methods. Chapter four is about the computations, as well as the results and ends with a discussion of the possible sources of errors. Chapter five concludes this work and contains and a brief outlook on what can be done in order to improve the method presented during the previous chapters. The Appendix contains the derivation of the topological charge and of the equation which is central to this work. Furthermore it will be explained in which way hadron masses have been computed.

# Chapter 2

# Theoretical Foundations

## 2.1 The $1+1-$Dimensional Schwinger Model ($QED_2$) with $N_f = 2$ Flavors of Fermions

### 2.1.1 The Schwinger Model in the Continuum

The Schwinger Model is a well known toy model for QCD since the theories share several interesting features with each other. In Euclidean space-time the Lagrangian of the model reads:

$$\mathcal{L}(\bar{\psi}, \psi, A_\mu) = \sum_{f=1}^{N_f} \bar{\psi}(x)^{(f)} \big(\gamma_\mu(\partial_\mu + igA_\mu(x)) + m\big)\psi(x)^{(f)} + \frac{1}{4}F_{\mu\nu}(x)F_{\mu\nu}(x). \qquad (2.1)$$

In a $1+1$-dimensional spacetime there are only three anti commuting $\gamma$ - matrices which can be realized in terms of the Pauli $\sigma$ matrices:

$$\gamma_1 = \sigma_1 = \begin{pmatrix} 0 & 1 \\ 1 & 0 \end{pmatrix}, \qquad \gamma_2 = \sigma_2 = \begin{pmatrix} 0 & -i \\ i & 0 \end{pmatrix} \qquad \gamma_5 = \sigma_3 = \begin{pmatrix} 1 & 0 \\ 0 & -1 \end{pmatrix}. \qquad (2.2)$$

The $U(1)$ gauge theory in two spacetime dimensions allows for topologically nontrivial configurations which are similar to instantons in 4-D Yang-Mills theory. Its low lying states contain a rather light iso-triplet which as "quasi-Nambu-Goldstone bosons" can be seen as the pions of this model [10]. One of the most important properties of the model is fermion confinement [11, 12]. Furthermore the Schwinger model is a super renormalizable theory which leads to an absence of the running coupling and hence the bare coupling $g$ does not need to be renormalized.

### 2.1.2 The Schwinger Model on the Lattice

In this work the Schwinger model (2.1) is simulated on a periodic spacetime lattice with $N_L^2$ lattice sites which corresponds to a spacetime extension of $L = N_L a$ where $a$ is the lattice spacing and $V = L^2$ the spacetime volume. As usual all dimensionless quantities are expressed in units of $a$ and denoted by a "$\hat{}$" symbol, e.g. the dimensionless gauge coupling reads $\hat{g} = ga$ and the dimensionless mass is $\hat{m} = ma$. One can approach the continuum limit by increasing $N_L$ while keeping the dimensionless ratios $gL = \hat{g}N_L$ and $M_\pi L = \hat{M}_\pi N_L$ fixed ($M_\pi$ denotes the mass of the aforementioned quasi Nambu-Goldstone bosons, i.e. the pion mass). This requires to decrease both $\hat{g}$ and $\hat{M}_\pi$ proportional to $1/N_L$ by sending $a \to 0$ (for the latter $\hat{m}$ has to be adjusted appropriately). In the Schwinger model on the lattice usually the dimensionless squared coupling constant $\beta = 1/\hat{g}^2$ is used instead of the coupling $\hat{g}$.

Furthermore the Wilson plaquette gauge action has been employed for this work

$$S_G[U] = \beta \sum_P \left[1 - \frac{1}{2}(U_P + U_P^\dagger)\right] = \beta \sum_P \left[1 - \text{Re } U_P\right] \ . \tag{2.3}$$

$U_P$ denotes an elementary plaquette which is given by a product of link variables

$$U_P = U_{n,1} U_{n+\hat{1},2} U^\dagger_{n+\hat{2},1} U^\dagger_{n,2}, \tag{2.4}$$

with the gauge links $U_{n,\mu} \in U(1)$

$$U_{n,\mu} = e^{i\hat{g}A_{n,\mu}} \ , \qquad U^\dagger_{n,\mu} = U_{n+\mu,-\mu}, \tag{2.5}$$

where $n$ labels the lattice sites with space-time coordinates $(x, t)$ and $\mu = 1, 2$ are the directions on the two dimensional lattice. Using eq.'s (2.3) - (2.5) $U_P$ can be expressed in terms of the discretized field strength tensor

$$U_P = e^{i\hat{g}a^2\hat{F}_{12}} \ , \tag{2.6}$$

with

$$\hat{F}_{12} = \frac{1}{a}\left(\left(A_2((n+\hat{1})a) - A_2(na)\right) - \left(A_1((n+\hat{2})a) - A_1(na)\right)\right) \tag{2.7}$$

which is relevant for the definition of the topological charge on the lattice presented in section 2.18.

### 2.1.3 Wilson Fermions

As briefly mentioned in the introduction all the simulations were performed with Wilson fermions which are quite cheap to simulate. The choice of Wilson fermions implies the use of the Wilson-Dirac operator. The gauge invariant expression for $N_f = 2$ flavors reads

$$D_W^{n,m} = (m_0 + 2r)\delta_{n,m} - \frac{1}{2}\sum_{\mu}\Big((r-\sigma_\mu)U_{n,\mu}\delta_{n,m-\hat{\mu}} + (r+\sigma_\mu)U^{\dagger}_{m,\mu}\delta_{n,m+\mu}\Big). \tag{2.8}$$

Thus the following gauge invariant action is obtained:

$$\begin{aligned} S_W =&(m_0 + 2r)\bar{\psi}_m\psi_m \\ &- \frac{1}{2}\sum_{\mu,m}\Big(\bar{\psi}_{m-\hat{\mu}}(r-\sigma_\mu)U_{m-\hat{\mu},\mu}\,\psi_m + \bar{\psi}_{m+\hat{\mu}}(r+\sigma_\mu)U^{\dagger}_{m,\mu}\,\psi_m\Big) \end{aligned} \tag{2.9}$$

For this work the Wilson parameter was chosen as $r = 1$. Due to the Wilson term an explicit chiral symmetry breaking occurs which causes the need for additive renormalization of the fermion mass according to

$$m_f = m_0 - m_c. \tag{2.10}$$

The bare fermion mass $m_0$ is the parameter to be chosen for simulations with Wilson fermions. The critical mass $m_c$ can be obtained by suitable extrapolations [13].

## 2.2 Topology in QED$_2$

### 2.2.1 Topological Charge in QED$_2$

This section gives a short presentation of topological charge. A much more detailed discussion, in particular for QED$_2$, can be found in [12]. The topological charge $Q$ which is an integer valued functional for classical, differentiable gauge fields can be seen as a winding number, carried by a pure gauge winding $Q-$times around a compactified space at time equal plus infinity. In QED$_2$ it is slightly different compared to the analog in 4D Yang-Mills theory.

The expression for the 2D $U(1)$ version is

$$Q \;=\; \frac{g}{4\pi}\int \mathrm{d}^2x\,\epsilon_{\mu\nu}\,F_{\mu\nu}\,, \tag{2.11}$$

with the field strength tensor

$$F_{\mu\nu} = \partial_\mu A_\nu - \partial_\nu A_\mu\;, \tag{2.12}$$

while the more complicated expression in the case of 4D $SU(2)$ reads

$$Q = \frac{g^2}{16\pi^2}\int \mathrm{d}^4x\,Tr(F_{\mu\nu}\tilde{F}_{\mu\nu}) \tag{2.13}$$

$$\text{with}\quad \tilde{F}_{\mu\nu} = \frac{1}{2}\epsilon_{\mu\nu\rho\sigma}F_{\rho\sigma}\quad\text{and}\quad F_{\mu\nu} = \partial_\mu A_\nu - \partial_\nu A_\mu - ig\,[A_\mu, A_\nu]. \tag{2.14}$$

The reason for the different expressions of both theories will become clear in the derivation of eq.(2.11), given in appendix A.1.

### 2.2.2 The Topological Charge on the Lattice

In order to investigate topological effects on the lattice a discretized version of the topological charge needs to be introduced. A suitable expression of a lattice topological charge is given by

$$Q = \frac{1}{2\pi}\sum_{n=0}^{N}\hat{F}_{12}(n), \tag{2.15}$$

where the sum runs over the vertices of the lattice. The field strength tensor (c.f. eq.(2.7)) represents the plaquette angle which is the sum over the values of the gauge field components assigned to an elementary plaquette with vertices labeled by $n$. This expression vanishes for periodic boundary conditions. For this reason one considers the imaginary part of the logarithm of the plaquette (c.f. eq.'s (2.4)-(2.7))

$$Q = \frac{1}{2\pi}\sum_n \mathrm{Im}\,\ln U_{12}(n) = \frac{1}{2\pi}\sum_n f\left(\left(A_{n+\hat{1},2} - A_{n,2}\right) - \left(A_{n+\hat{2},1} - A_{n,1}\right)\right), \tag{2.16}$$

where

$$\mathrm{Im}\,\ln U_{12}(n) = \phi_{P,n}$$

is the plaquette angle which is restricted to $\phi_{P,n} \in [-\pi, \pi]$ by the function $f$ with

$$f(x) = x - \text{floor}\left(\frac{x+\pi}{2\pi}\right) 2\pi \,, \qquad x \in [-4\pi, 4\pi]. \tag{2.17}$$

The function $f(x)$ ("floor" means rounding to the next lower integer value) repeatedly adds $2\pi$ to $x$ until the result is in $[-\pi, \pi]$. This projection is visualized in figure 2.1.

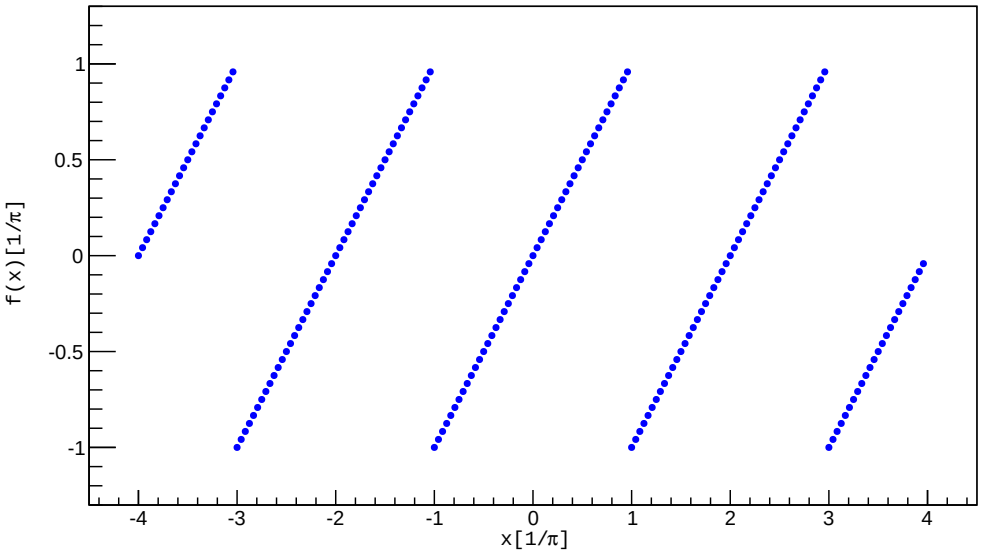


FIGURE 2.1: The function $f(x) = x - \text{floor}\,((x+\pi)/(2\pi))\,2\pi$ projects $x \in [-4\pi, 4\pi]$ into the interval $[-\pi, \pi]$.

Thus the lattice version of the topological charge reads:

$$Q = \frac{1}{2\pi} \sum_n \phi_P(n)\,, \quad \text{with} \quad -\pi < \phi_P(n) < +\pi\,. \tag{2.18}$$

This definition is also referred to as the geometrical definition [14, 15].

## 2.3 Physical Hadron Masses from Computations in Fixed Topological Sectors

As mentioned before (c.f. chapter 1) simulating at fine lattice spacings leads to fixed topology. In this case a theory is non-local and has no Hamiltonian. Hence it does not correspond to a physical theory. As a consequence observables are plagued by systematic effects. The dependency of observables on topological charge has been understood analytically and a formulae has been derived which allows to reliably extrapolate to the physical limit [6, 7]. As a starting point the path integral can be decomposed into topological sectors. This can be done by introducing the $\theta$ parameter. In Appendix A.2 it is shown how the $\theta$-term leads to fixed topology. Besides the technical character, the $\theta$ parameter has the more profound and physical meaning of a $\theta$-vacuum which, as a quantum state, is the superposition of topological sectors. A discussion about the $\theta$-vacuum in great detail can be found in [12].

A general 2-point correlation function $C_{Q,V}$ of hadron creation operators $O_i$ at a fixed topological sector reads

$$\begin{aligned} C_{Q,V} &= \langle O_1 O_2 \rangle && (2.19)\\ &= \frac{1}{Z_{Q,V}} \frac{1}{2\pi} \int_{-\pi}^{\pi} \mathrm{d}\theta \, e^{i\theta\nu} \int \mathrm{D}[U] \, O_1 O_2 \, e^{-S_{eff}[U] - i\theta Q[U]} && (2.20)\\ &= \frac{1}{Z_{Q,V}} \frac{1}{2\pi} \int_{-\pi}^{\pi} \mathrm{d}\theta \, Z(\theta) \, C(\theta) \, e^{i\theta Q}, && (2.21) \end{aligned}$$

with

$$C(\theta) = \int \mathrm{D}[U] \, O_1 O_2 \, e^{-S_{eff}[U] - i\theta\nu[U]}. \tag{2.22}$$

For a sufficiently large space-time volume $V$ a saddle point approximation can be used and the correlation function

$$C_{Q,V}(t) = A_{Q,V} \, e^{-M_{Q,V} \, t} \tag{2.23}$$

can be expanded in the parameters $M''(0)\, t/V\, \chi_t$, $1/V\, \chi_t$ and $Q^2/V\, \chi_t$, in order to obtain

$$M_{Q,V} = M(0) + \frac{1}{2} M''(0) \, \frac{1}{V\chi_t} \left( 1 - \frac{Q^2}{V\chi_t} \right) + \mathcal{O}\left( \frac{1}{V^2} \right). \tag{2.24}$$

This expression represents one of the central equations used in this work. For a detailed derivation see appendix A.2.

The expression contains the following quantities:

- $M_{Q,V}$ is the hadron mass excited by a suitable operator $O$ at fixed topological charge $Q$ in a finite space-time volume $V$.
- $M(0)$ is the $\theta$-dependent physical hadron mass at infinite space-time volume $V$ at $\theta = 0$.
- $M''(0)$ is the second derivative of $M(\theta)$ with respect to $\theta$, i.e. $M''(0) = d^2M(\theta)/d\theta^2|_{\theta=0}$.
- $\chi_t$ is the topological susceptibility which is given by

$$\chi_t = \lim_{V\to\infty} \frac{\langle Q^2 \rangle}{V}. \tag{2.25}$$

Eq. (2.24) shows that fixing topology induces finite size effects. The infinite volume limit $V \to \infty$ renders all topological sectors equally such there is no difference between $M_{Q,V}$ and $M(0)$. In order to determine physical hadron masses from fixed topology computations a method will be presented in chapter 4 which has been proposed in [6] and tested in [8, 9]. This method consists of two steps:

1. Perform simulations at fixed topology for different topological charges Q and space-time volumes $V$, for which the expansion (2.23) and (2.24) is a good approximation. This means the parameters $M''(0)\, t/V\, \chi_t$, $1/V\, \chi_t$ and $Q^2/V\, \chi_t$, must be sufficiently small. From the simulations determine the masses $M_{Q,V}$ according to (2.23).
2. By fitting (2.24) to the masses $M_{Q,V}$ obtained in step one the physical hadron mass $M(0)$, $M''(0)$ and $\chi_t$ can be determined.

# Chapter 3

# The Simulation Algorithm

This chapter presents in a concise way the Hybrid Monte Carlo algorithm which has been used in order to simulate the Schwinger model on the lattice. The presentation includes a discussion of the implemented optimization methods which allow for significant speed ups in terms of the simulation time. For a more detailed discussion on this particular HMC and its optimizations see [13].

## 3.1 The Basic Principle of the HMC

The purpose of the simulations is to compute the expectation value of e.g. correlation functions by averaging over a sufficiently large number of gauge link configurations. To this end the Schwinger model with $N_f = 2$ flavors of fermions has been simulated by using the HMC algorithm with pseudofermions and the conjugate gradient algorithm for the inversion of the fermion matrix $Q^2 = \gamma_5 D_W \gamma_5 D_W$ which is hermitian and positive definite.

The HMC algorithm combines the concepts of Molecular Dynamics and Monte Carlo Simulations and is based on randomly generating gaussian distributed conjugate momenta $P_i$ to the field variables $X_i$ such that the Hamiltonian of the system assumes the form of

$$\mathcal{H}(X,P) = \frac{1}{2}\sum_i P_i^2 + S[X], \tag{3.1}$$

where $\mathcal{H}$ is conserverd under the equations of motion (EOM's):

$$\dot{X}_i = \frac{\partial \mathcal{H}}{\partial P_i}\,, \qquad \dot{P}_i = -\frac{\partial \mathcal{H}}{\partial X}. \tag{3.2}$$

This approach is also known as molecular dynamics approach. By integrating the EOM's along a trajectory a global update $(X, P) \longrightarrow (X', P')$ is generated, where $(X, P)$ and $(X', P')$ are points on the surface of a subspace of a phase space. On the surface of this phase space the energy is conserved and does only change by the reason of numerical errors which occur due to the integration. The change in the energy which is given by $\Delta\mathcal{H} = \mathcal{H} - \mathcal{H}'$ depends on the step size $\Delta\tau$ chosen for the integration along the virtual time trajectory $\tau$. Such a global update gets accepted with the probability of

$$\mathcal{P}((X, P) \longrightarrow (X', P')) = \min\left(1, e^{\mathcal{H}(X,P)-\mathcal{H}(X',P')}\right). \tag{3.3}$$

For the simulations performed for this work the length of the trajectory was chosen as $\tau = 1$ and the step size $\Delta\tau$ was adjusted such that each time an acceptance rate for the new field configurations of approximately 80% could be reached.

## 3.2 Optimization Methods

Depending on the choice of the fermion mass $\hat{m}_0$, the value of $\beta$ and the number of field configurations being generated, the invested computation resources of the simulations can be considerably non-negligible even for a more simple theory such as $\mathrm{QED}_2$. Therefore the HMC being used works with several optimization methods. These will briefly be explained below. For more details on this topic see [13, 26].

### 3.2.1 The Integration Scheme

The first noteworthy technicality is the Leapfrog integration scheme which is not just implemented in particular in the HMC used for this work but usually in this type of Monte Carlo algorithms in general. The Leapfrog integration scheme has the property of symplecticity which implies reversibility and area preservation. Furthermore this property causes the change in the energy to be independent of the trajectory length. Instead the change in the energy does only depend on the step size. The process of this integration consists of two types of update steps

$$T_A(\Delta\tau): \quad A_{n,\mu} \to A'_{n,\mu} = A_{n,\mu} + \Delta\tau P_{n,\mu}\,, \tag{3.4}$$

$$T_S(\Delta\tau): \quad P_{n,\mu} \to P'_{n,\mu} = P_{n,\mu} - \Delta\tau \frac{\partial S[A,\eta]}{\partial A_{n,\mu}}\,, \tag{3.5}$$

resulting in a basic Leapfrog time evolution step

$$T_{L_i} = T_S(\Delta\tau/2)\, T_U(\Delta\tau)\, T_S(\Delta\tau/2). \tag{3.6}$$

Hence for a trajectory length $\tau$ the time evolution step $T$ gets successively applied $N_{MD}$ times where $N_{MD} = \tau/\Delta\tau$ denotes the number of steps done along a trajectory $\tau$.

### 3.2.2 Multiple Time Scale Integration

Further performance optimizations can be achieved by integrating the action (see eq.(3.1)) on multiple time scales. This is based on the idea of splitting the action into several components:

$$\mathcal{H} = \frac{1}{2}\sum_{n,\mu} P_{n,\mu}^2 + \sum_{i=0}^{k} S_i[U]. \tag{3.7}$$

Each $S_i$ must be integrated separately whereat the integration of $S_i$ depends on the integration of $S_{i-1}$. The time evolution step for $S_0$ reads

$$T_{L_0} = T_{S_0}(\Delta\tau_0/2)\, T_U(\Delta\tau_0)\, T_{S_0}(\Delta\tau_0/2), \tag{3.8}$$

whereas the time evolution steps $T_i$ for the components $S_i$ with $i \neq 0$ are defined recursively:

$$T_i = T_{S_i}(\Delta\tau_i/2)\, [T_{i-1}]^{N_{i-1}}\, T_{S_i}(\Delta\tau_i/2). \tag{3.9}$$

The step sizes $\Delta\tau_i$ are given by

$$\Delta\tau_i = \frac{\tau}{\prod_{j=i}^{k} N_j} = \frac{\tau}{N_{MD_i}}. \tag{3.10}$$

The choice of the $N_j$ individually depends on the cost of the application of $T_{S_i}$ and also on the absolute value of the force defined by

$$F_i = \sqrt{\sum_{n,\mu} \left| \frac{\partial S_i[A,\eta]}{\partial A_{n,\eta}} \right|^2}. \tag{3.11}$$

In ref.[13] a splitting of the force into three components $S_0 := S_G,\ S_1 := S_{PF_1},\ S_2 := S_{PF_2}$ with two time scales was considered a good choice and is adopted for the simulations performed in this work. The values for the time scales were set to $N_1 = 1$ and $N_0 = 12$. In certain cases a reduction by approximately a factor of three of the simulation time could be observed.

### 3.2.3 Mass-Preconditioning

By decreasing the quark mass the condition number $\kappa$ of the fermion matrix $Q^2$ increases which leads to a larger number of iterations in the CG process. This effect can be counteracted by rewriting the squared determinant of the Dirac operator (appears when the fermonic part of the action is integrated out for $N_f = 2$ flavors of fermions) according to:

$$(\det(D_W))^2 = \det(Q^2) = \det(W^+W^-)\frac{\det(Q^2)}{\det(W^+W^-)}. \tag{3.12}$$

$W^+$ and $W^-$ are fermonic fields being chosen such that $W^+W^-$ approximates $Q^2$ but is less expensive to convert for the CG algorithm. For the HMC being used in this work these fermonic fields were chosen as $W^+ = Q + i\mu$ and $W^- = (W^+)^\dagger = Q - i\mu$ [13]. Hence the product of the fields is $W^+W^- = Q^2 + \mu^2$. An appropriate choice for $\mu^2$ in order to keep the condition number of both operators small is $\mu^2 = \sqrt{\lambda_{max}(Q)\lambda_{min}(Q)}$ which leads directly to

$$C\left(Q^2 + \mu^2\right) \approx \frac{\lambda_{max}(Q)}{\mu^2} = \sqrt{C\left(Q^2\right)}. \tag{3.13}$$

as well as

$$C\left(\left(Q^2 + \mu^2\right)^{-1} Q^2\right) \approx \frac{\mu^2}{\lambda_{min}(Q)} = \sqrt{C\left(Q^2\right)}. \tag{3.14}$$

By using the method of mass-preconditioning the simulation performance can be directly increased to a large degree by a proper adjustment of the parameter $\mu^2$. Instead of determining the eigenvalues of $Q^2$ , which is quite complicated, the value for $\mu^2$ is chosen such that the ratio of the absolute values of the forces caused by $S_1$ and $S_2$ is similar to the ratio of the corresponding applied operators. For the simulations done in this work a value for the ratio of the forces of $F_1/F_2 \approx N_1 = 1$ is obtained (c.f. section 3.2.2). For most of the simulations which were performed for values of $\beta = 3.0\,, 4.0$ and of pion masses $\hat{M}_\pi \approx \{0.2, ..., 0.3\}$ the values chosen for $\mu^2$ were closely distributed around $\mu^2 = 1$.

# Chapter 4

# Computations and Results

## 4.1 Topology Freezing

Using the HMC algorithm presented in the previous chapter simulations at various values of $\beta$, $\hat{m}$ and $N_L$ were performed. In figure 4.1 the probability for a transition to another topological sector per HMC trajectory is plotted versus $\hat{g} = 1/\sqrt{\beta}$ and $\hat{m}/\hat{g} = \hat{m}\sqrt{\beta}$, while $gL = \hat{g}N_L = N_L/\sqrt{\beta} = 24/\sqrt{5}$ is kept constant. $\hat{g}$ is proportional to the lattice spacing $a$. $\hat{m}/\hat{g}$ is proportional to $\hat{m}/a$ and, therefore, proportional to $m$, the bare quark mass in physical units. As expected there are frequent changes of the topological sector at large values of the lattice spacing $a$ (large values of $\hat{g}$), while at small values of $a$ (small values of $\hat{g}$) topology freezing is observed. The dependence of the probability for a transition on the bare quark mass $\hat{m}/\hat{g}$ is rather weak.

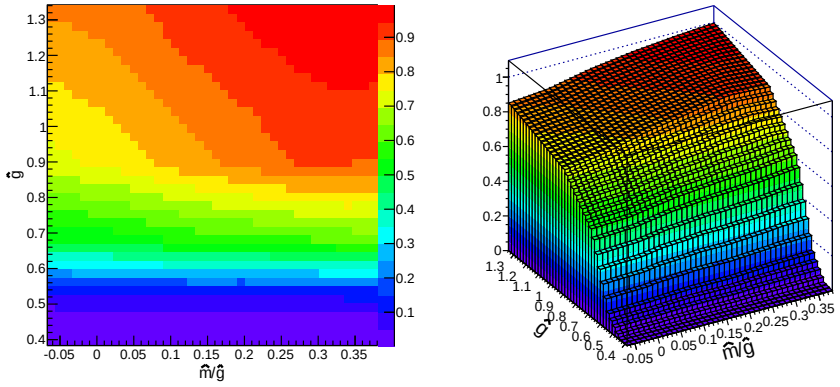


FIGURE 4.1: The probability for a transition to another topological sector per HMC trajectory as a function of $\hat{g} = 1/\sqrt{\beta}$ and $\hat{m}/\hat{g} = \hat{m}/\sqrt{\beta}$.

## 4.2 Computations at Fixed Topology

In the following discussion only dimensionless quantities are included. For reasons of convenience and readability the "ˆ" symbol will be omitted throughout the subsequent sections.

The hadron masses being investigated are the mass of the light isotriplet (will be considered as the pion mass $M_\pi$) and the static potential $\mathcal{V}_{\bar{q}q}(r)$ (the ground state energy of a static quark antiquark pair at separation $r$). The Operator used for the light isotriplet is

$$O_\pi \quad = \quad \sum_x \bar{\psi}^{(u)}(x)\gamma_1\psi^{(d)}(x) \tag{4.1}$$

($\sum_x$ denotes a sum over space and $u$ and $d$ label the two degenerate fermion flavors). In order to compute the corresponding correlation function the so called "one-end trick" method has been used [20]. For the static potential a suitable hadron creation operator is

$$O_{\bar{q}q} \quad = \quad \bar{q}(x_1)U(x_1,x_2)q(x_2) \quad , \quad r \quad = \quad |x_1 - x_2|, \tag{4.2}$$

where $\bar{q}$ and $q$ represent scalar static color charges and $U(x_1, x_2)$ is the product of spatial links connecting $x_1$ and $x_2$ for which the implementation is straightforward.

The hadron masses $M_{Q,V} \equiv M_{\pi,Q,V}$ and $M_{Q,V} \equiv \mathcal{V}_{\bar{q}q,Q,V}(r)$ (c.f. eq.(2.24)) are obtained at fixed topology by first determining the topological charge $Q$ on each gauge link configuration according to (2.18). Then independent computations of the pion mass and the static potential are performed using only gauge link configurations with the same absolute value of $Q$. The pion mass as well as the ground state energy from the static potential have been computed by fitting effective mass plateaus. For a more detailed explanation on how the masses are extracted and computed from correlation functions see A.3.

To check the quality of the results presented in the subsequent sections, it will be necessary to have a reference value for the hadron mass and for the dimensionless topological susceptibility $\chi_t$. These will be obtained in the conventional way. For the hadron mass $M^{\text{conv}}$ this means i.e. computing the corresponding temporal correlation function on all available gauge link configurations (i.e. as an average over all topological sectors) at a single sufficiently large $V$ (to avoid ordinary finite size effects). The topological susceptibility is computed from the topological charge distribution according to eq.(2.25).

The computations are performed for a choice of $\beta = 3.0$ , $m_0 = -0.07$ and $\beta = 4.0$ , $m_0 = -0.03$, which assures sufficiently many transitions between different topological sectors (c.f. figure 4.1), to safely determine the hadron mass and the topological susceptibility in the conventional way. In this case the topological charge distribution must be gaussian [21] which is fulfilled for the considered choice of parameters. For $\beta = 3.0$ the topological charge distribution has been visualized by a histogram and is shown in figure 4.2. The error of $\chi_t$ has been computed by using the Jackknife method.

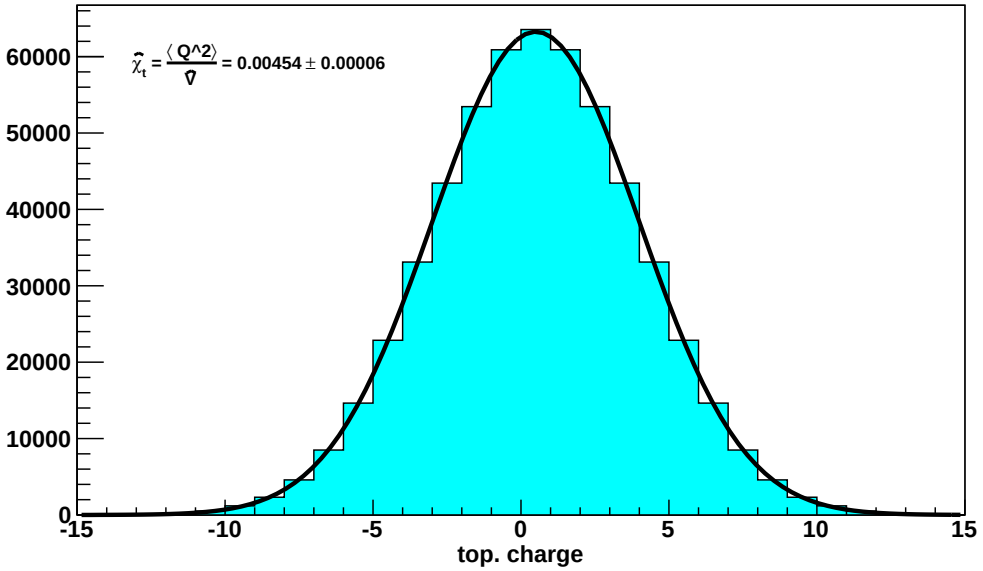


FIGURE 4.2: The topological charge distribution for $\beta = 3.0$ , $m_0 = -0.07$ , $N_L = 52$. $\chi_t$ has been computed according to $\chi_t = \lim_{V\to\infty}\langle Q^2\rangle/V$. The vertical axis corresponds to the number of configurations. The horizontal axis corresponds to the topological sectors.

For the computation of the hadron masses all of the configurations generated during the simulations have been used. Autocorrelation effects are rather weak for the chosen parameters which is consistent with the fact that there are sufficiently many topological charge transitions. To fully avoid these effects at first the integrated autocorrelation time has been computed according to

$$\tau = \frac{1}{2} + \frac{\sum_n \Gamma(n)}{\Gamma(0)}, \tag{4.3}$$

$$\Gamma(n) = \frac{1}{N-n} \sum_{i=1}^{N-n} ( C_i(t) - \langle C(t)\rangle ) ( C_{i+n}(t) - \langle C(t)\rangle ). \tag{4.4}$$

In this expression $C_i(t)$ is the correlation function computed from configuration $i$. $\langle C(t)\rangle$ is the mean value which is obtained by averaging over all $N$ configurations. Afterwards the configurations are binned with a sufficiently large bin size which is $\geq \tau$.

### 4.2.1 The Strategy

In the following the lattice results of the masses $M_{Q,V} \equiv M_{\pi,Q,V}$ and $M_{Q,V} \equiv \mathcal{V}_{\bar{q}q,Q,V}(r)$ are plotted against $1/V = 1/N_L^2$. The hadron mass $M(0)$ in the infinite volume limit at $\lim_{V\to\infty} 1/V = 0$ as well as the topological susceptibility $\chi_t$ are obtained according to the description given in section 2.3 and eq.(2.24). As discussed before eq.(2.24) is an expansion in $M''(0)t/\chi_t V$, $1/\chi_t V$ and $Q^2/\chi_t V$. Therefore, only fixed topology masses $M_{Q,V}$ with sufficiently small values of $1/\chi_t V$ and $Q^2/\chi_t V$ should be included in the fit. In the presented fits the information about the expansion parameters is included by computing the following expression for each topological sector:

$$x_Q = \min\left( \frac{1}{V_{\min}^Q \chi_t} \, , \, \frac{Q^2}{V_{\min}^Q \chi_t} \right) \tag{4.5}$$

The parameter $1/V_{\min}^Q \chi_t$ is considered in the case of $Q = 0$ whereas the parameter $Q^2/V_{\min}^Q \chi_t$ is considered for $Q \neq 0$. Only the lowest volume $V_{\min}$ in $x_Q$ is of particular interest since this is the delimiting factor for the accuracy of the fit. A first illustration for such a fit of the pion mass is shown in figure 4.3. In this figure each curve $M_{\pi,Q}(V)$ represents a different topological sector. The corresponding volumes are marked on the $1/V$-axis. Consider, for example, the point $M_{\pi,Q=3}\left(V = 24^2\right)$ in figure 4.3. The corresponding $x_Q = 3.44$ is computed according to eq.(4.5). In this example the values of the discussed parameters are rather large and therefore the validity is quiet questionable. This is reflected by the mass $M(0) = 0.2650(1)$ obtained from the fit which deviates from the reference value $M_\pi^{\text{conv}} = 0.2664(2)$ by $12\sigma$ and hence is inconsistent. The fit parameter $\chi_t = 0.00161(16)$ deviates from the reference value ${\chi_t}^{\text{tcd}} = 0.00454(6)$ ("tcd" denotes "topological charge distribution") computed from the topological charge distribution (c.f. figure 4.2) by $\approx 18\sigma$ leaving the result inconsistent, too. The expansion parameters have to be further restricted to smaller values.

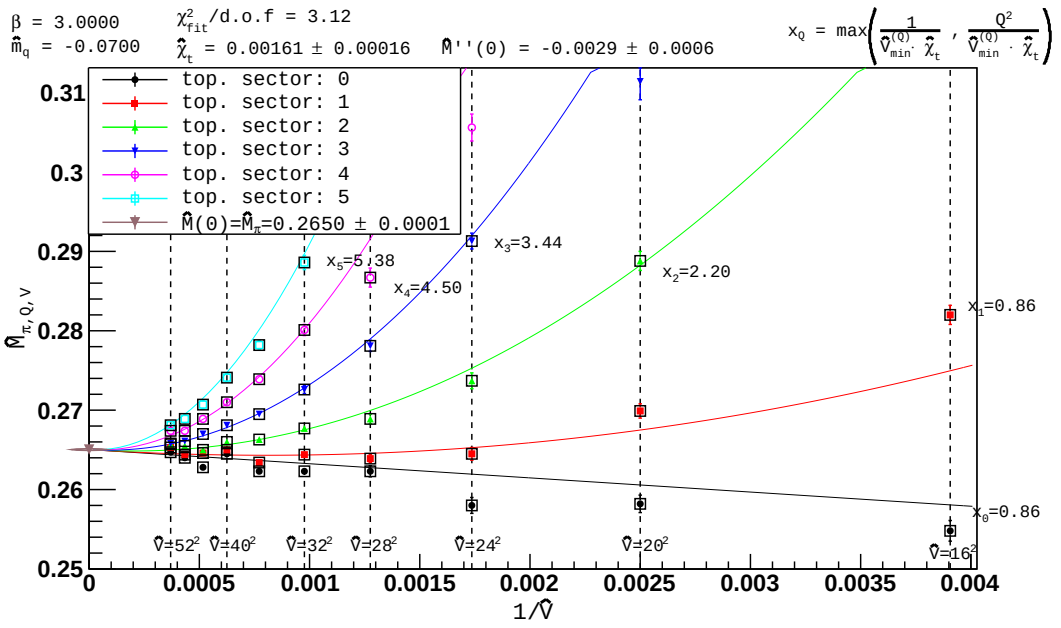


FIGURE 4.3: Hadron mass extrapolation for $\beta = 3.0$, $m_0 = -0.07$, $V = \{16^2, \ldots, 52^2\}$. $x_Q$ is not sufficiently small in order to guarantee the validity of the fit. Reference value for the pion mass $M_\pi^{\text{conv}} = 0.2664(2)$ and for the topological susceptibility $\chi_t = 0.00454(4)$.

Though it cannot be said a priori what exactly "small" or "large" means concerning the value of $x_Q$ and $|M''(0)|t/V\chi_t$. For the latter this seems quite unproblematic and it can be checked by simply computing $|M''(0)|t/V\chi_t$ for each data point $M_{Q,V}$. The parameter $|M''(0)|$ was never $\geq 0.09$. The smallest volume taken into account for the fits is $V = 28^2$ and the corresponding maximal time for fitting a mass plateau to obtain $M_{Q,V}$ is $n_t = 13$. The value of $\chi_t^{\text{tcd}}$ for $\beta = 4.0$ and $m_0 = -0.03$ is $\chi_t^{\text{tcd}} \approx 0.00353$. This leads to a value for the expansion parameter of $M''(0)t/V\chi_t \approx 0.42$ which seems to be sufficiently small.

For $x_Q$ the investigations have shown that in most of the cases a value of $x_Q \approx 2.5$ should not be exceeded because then the results become inconsistent. Further lowering of this value should improve the fit results since the expansion given by eq.(2.24) becomes more precise. Lowering this value can be achieved by excluding masses $M_{\pi,Q,V}$. It seems reasonable to choose a certain value $x_Q^{\text{b}}$ that should not be exceeded. Then the fit will be repeated multiple times and for each subsequent fit the masses $M_{\pi,Q,V}$ are excluded as follows:

1. Consider the curve $M_{\pi,Q}(V)$ describing the mass in the topological sector $Q$ as a function of the space-time volume $V$.

2. Start by excluding the mass $M_{\pi,Q,V_{\min}}$ belonging to the minimum volume and perform the fit.

3. Repeat steps (1) and (2) for each curve $M_{\pi,Q}(V)$ as long as $x_Q > x_Q^b$.

Applying these steps for the fit done in figure 4.3 leads to the result shown in figure 4.4.

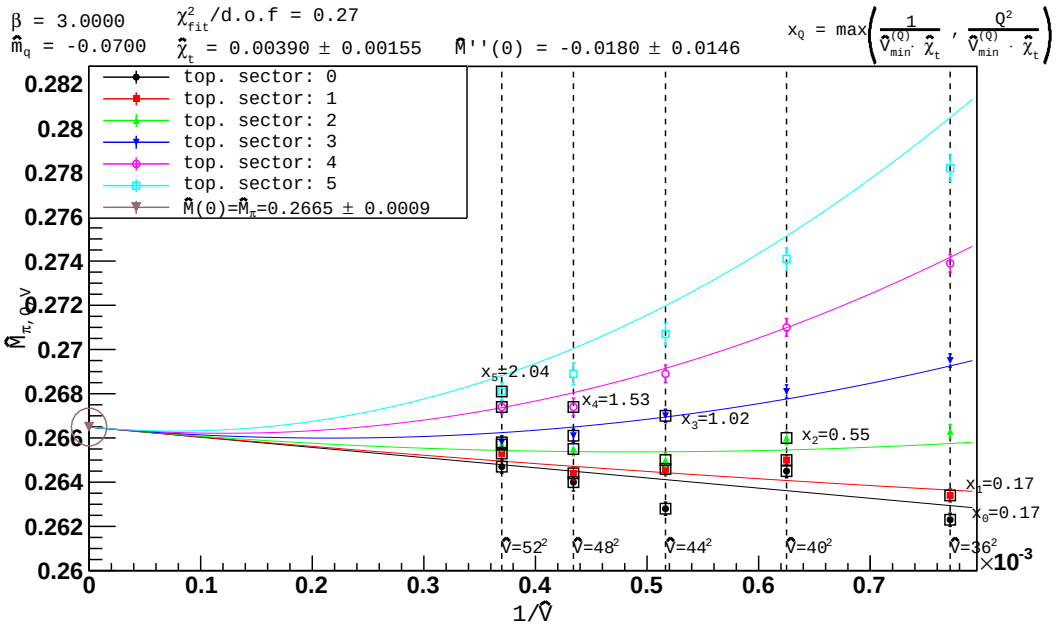


FIGURE 4.4: Hadron mass extrapolation for $\beta = 3.0$, $m_0 = -0.07$, $V = \{36^2, \ldots, 52^2\}$. Certain $M_{\pi,Q_i,V_{\min}}$ were excluded such that $x_Q$ is restricted to $x_Q \lesssim 2.0$. Reference value of the pion mass $M_\pi^{\text{conv}} = 0.2664(2)$ and of the topological susceptibility $\chi_t = 0.00454(4)$

Now the mass $M(0)$ and the topological susceptibility show consistency with the reference values. A further discussion about the results will be given in the subsequent chapters. However, for many cases it turned out that rigidly following the description given above can be disadvantageous. For some fits this means trying to lower the value of $x_Q$ by excluding masses $M_{Q,V}$ from the fit yields no additional improvement or even worsens the fit results. The reason for this might be systematic errors which can occur during the determination of the masses $M_{\pi,Q,V}$ by fitting a constant to an effective mass plateau with large statistical errors (see section 4.3 about error discussion).

Another issue is the value of the fit parameter $\chi_t$ which due to the mentioned systematic errors can strongly fluctuate when excluding the masses $M_{Q,V}$ from the fit. Then computing $x_Q$ with the fit parameter $\chi_t$ can result in a larger $x_Q$, instead of a

lower one. In order to estimate the systematic errors different heuristic methods for choosing the data points will be tested and compared.

The basic strategy will be to perform the fit while keeping $x_Q$ below certain values. As upper limits the values $x_Q^{\mathrm{b}} = \{0.5, 1.0, 1.5, 2.0, 2.5\}$ are explored. In this sense performing a fit for e.g. $x_Q^{\mathrm{b}} = 1.5$ means trying to keep $x_Q \lesssim 1.5$. For the fitting procedure four different strategies will be adopted:

a) Using the fitted parameter $\chi_t$ for the determination of $x_Q$.

b) Using $\chi_t^{\mathrm{tcd}}$ for the computation of $x_Q$, making it independent of the fitted $\chi_t$.

c) A rather heuristic approach which describes a strict selection rule of the masses $M_{Q,V}$ to be included in the fit and has proved to yield acceptable results: The topological sectors included in a fit shall be denoted by $Q_0, \ldots, Q_N$ with $(Q_1 \leq Q_i < Q_N)$ and the volumes included for each topological sector by $V_0^{(Q_i)}, \ldots, V_N^{(Q_i)}$ with $(V_0^{(Q_i)} \leq V_n^{(Q_i)} < V_N^{(Q_i)})$. The parameter $x_{Q_i}$ is chosen such that $V_0^{(Q_{i+1})} = V_{0+1}^{(Q_i)}$ and $V_0^{(Q_1)} = V_0^{(Q_0)}$. This approach has already been used for the fits of figure 4.3 and 4.4.

d) Using strategy c) and additionally using $\chi_t$ computed from the topological charge distribution as a fixed fit parameter in order to see if a further stabilization of the fit can be achieved.

In the following sections, fit results for the pion mass and for the static $q\bar{q}$ potential with two different sets of parameters each are summarized in tables. The results obtained by adopting strategies a) - d) for the fits will be discussed in detail for the pion mass and the parameters $\beta = 3.0$ , $m_0 = -0.07$ , $N_L = \{28, ..., 52\}$.
For the subsequent discussions about the results the strategies a) and b) are dropped since the results seem to have a bad precision.

The presented tables are structured in the following way: The fits are labeled by numbers and the corresponding strategies (c.f. 4.2.1: Strategies a-d). $x_Q^{\max}$ denotes the largest $x_Q$ of the fit. Further quantities that are given in the table are $M(0)$ (obtained from the fit; corresponds to the hadron mass at unfixed topology), $M^{\mathrm{conv}}$, $\chi_t$ (obtained by the fit) and $\chi_t^{\mathrm{tcd}}$.

In many cases no further restriction on the value of $x_Q$ is imposed because this leads to significantly worse results. The reason for this might be the errors of $M_{Q,V}$ or the absence of a sufficient number of data points. This issue will be discussed in section 4.3.

### 4.2.2 Results for the Pion Mass

In table 4.1 it can be seen that for strategies a) and b) the restriction of $x_Q$ tends to bring $M(0)$ closer to $M_\pi^{\text{conv}}$. For the case of b) the value of $x_Q^{\max}$ must be restricted to 0.9 until a fit result could be reached which is consistent with the reference value within $1\sigma$. In order to reach the same deviation for b) the value of $x_Q^{\max}$ had to be restricted to $x_Q^{\max} = 0.38$. Further lowering of $x_Q^{\max}$ as it is done for fit no. 7 preserves the consistency of the result but the statistical error is quite large. This can be explained by the smaller number of masses $M_{\pi,Q,V}$ taken into account for the fit. The discrepancy between a) and b) concerning the values of $x_Q$ seems not surprising since, as explained above, for a) the value of $x_Q$ depends on the fit parameter $\chi_t$ which is strongly fluctuating among the different fits which is a drawback compared to b).

For both approaches the fitted $\chi_t$ cannot reach consistency with the reference value $\chi_t^{\text{tcd}} = 0.00454(6)$. For a) the fitted value deviates by $\approx 5\sigma$ (fit no. 4) and for b) by $\approx 4\sigma$ (fit no. 6). Even for low values of $x_Q$ (e.g. when a consistency of the hadron mass is achieved) method a) and b) seem not to be suited for the determination of $\chi_t$. The reason for this remains unclear but it can be assumed that the low precision is caused by systematic errors.

| strategy | Nr. | $\chi^2$/dof | $x_Q^{\max}$ | $M(0)$ | $M_\pi^{\text{conv}}$ | $\chi_t^{\text{fit}}$ | $\chi_t^{\text{tcd}}$ |
|---|---|---|---|---|---|---|---|
| a) | 1 | 0.92 | 2.15 | 0.2652(2) | 0.2664(2) | 0.00182(24) | (no input) |
| | 2 | 0.93 | 1.75 | 0.2656(2) | | 0.00190(23) | |
| | 3 | 0.51 | 1.45 | 0.2655(3) | | 0.00173(22) | |
| | 4 | 0.39 | 0.90 | 0.2662(4) | | 0.00229(43) | |
| b) | 1 | 1.64 | 2.39 | 0.2654(2) | 0.2664(2) | 0.00226(23) | 0.00454(6) |
| | 2 | 1.21 | 2.04 | 0.2654(2) | | 0.00214(26) | |
| | 3 | 1.01 | 1.53 | 0.2656(2) | | 0.00223(28) | |
| | 4 | 0.79 | 1.02 | 0.2651(2) | | 0.00176(23) | |
| | 5 | 0.70 | 0.55 | 0.2657(3) | | 0.00184(22) | |
| | 6 | 0.33 | 0.38 | 0.2659(6) | | 0.00192(67) | |
| | 7 | 0.33 | 0.17 | 0.2671(14) | | 0.00189(101) | |

TABLE 4.1: Pion mass results for $\beta = 3.0$, fermion mass $m_0 = -0.07$ and $N = \{28, \ldots, 52\}$

In table 4.2 for the case of c)-1 and 2, $M(0)$ of the first fit is slightly more precise compared to fit nr. b)-6 whereas c)-2 comes with a slightly larger statistical error. There is no huge improvement compared to a) and b), if at all.

Though what can be observed is that results of similar precision are already obtained at larger $x_Q$. The fitted $\chi_t$ is much closer to the reference value compared to the fitted $\chi_t$ from a) and b) but with a very large statistical error with an average of approximately 60%. Having tested strategies a) - d) the low precision suggests that for the used operators the method is not suited for the determination of $\chi_t$ by performing fits on single data sets (one observable at a time).

Nevertheless the selection of $M_{\pi,Q,V}$ used in order to perform these fits could be interesting for the simultaneous fitting of multiple data sets (data of different observables) which will be discusses in section 4.2.4 where the idea is to stabilized the fit and hence to reduce the statistical error on $\chi_t$ by fitting a larger data set.

Since $\chi_t$ seems to be very problematic and influences the results for $M(0)$ (c.f. eq.(2.24)), the question arises if further improvements for the fitted hadron mass can be achieved. Therefore strategy d) is tested, for which $\chi_t$ is used as a fixed parameter for the fit. The masses $M_{\pi,Q,V}$ are excluded as in c). The first two fits for d) show indeed a slight improvement with a lower statistical error compared to the results achieved by using strategies a), b) and c). For lower values of $x_Q$ (see fits nr. 3-5) they stay consistent but the statistical error increases which again can be explained by the smaller number of masses being fitted.

| strategy | Nr. | $\chi^2$/dof | $x_Q^{\max}$ | $M(0)$ | $M^{\text{conv}}$ | $\chi_t^{\text{fit}}$ | $\chi_t^{\text{tcd}}$ |
|---|---|---|---|---|---|---|---|
| c) | 1 | 0.42 | 2.39 | 0.2662(5) | 0.2664(2) | 0.00352(99) | 0.00454(6) |
| | 2 | 0.27 | 2.04 | 0.2665(9) | | 0.00390(155) | |
| | 3 | 0.15 | 1.30 | 0.2657(16) | | 0.00292(396) | |
| | 4 | 0.17 | 0.73 | 0.2669(27) | | 0.00498(251) | |
| | 5 | 0.05 | 0.33 | 0.2683(28) | | 0.00500(341) | |
| d) | 1 | 0.44 | 2.39 | 0.2666(2) | 0.2664(2) | (fixed) | 0.00454(6) |
| | 2 | 0.26 | 2.04 | 0.2668(4) | | | |
| | 3 | 0.15 | 1.30 | 0.2662(8) | | | |
| | 4 | 0.15 | 0.73 | 0.2667(11) | | | |
| | 5 | 0.04 | 0.33 | 0.2681(26) | | | |

TABLE 4.2: Pion mass results for $\beta = 3.0$, fermion mass $m_0 = -0.07$ and $N = \{28, \ldots, 52\}$

From the foregoing discussion it can be concluded that the approaches c) and d) are most promising. Therefore the following discussion will be restricted to these ones. In table 4.3 the fits c)-1 and d)-1 show quite precise results. c)-1 is slightly superior to d)-1.

In both cases after lowering $x_Q$, the value of $M(0)$ is less precise but due to an increase in the statistical error the consistency with the reference value $M_\pi^{\text{conv}}$ is preserved. For the fit performed with c) the value of $M(0)$ is very close to the reference value and the statistical error is quiet small, too. For the case of $\beta = 4.0$ there is no improvement in the precision for $\chi_t$ compared to $\beta = 3.0$.

| strategy | Nr. | $\chi^2$/dof | $x_Q^{\max}$ | $M(0)$ | $M^{\text{conv}}$ | $\chi_t^{\text{fit}}$ | $\chi_t^{\text{tcd}}$ |
|---|---|---|---|---|---|---|---|
| c) | 1 | 2.03 | 3.07 | 0.2742(4) | 0.2743(3) | 0.00314(34) | 0.00353(14) |
| | 2 | 0.96 | 2.62 | 0.2749(10) | | 0.00403(133) | |
| d) | 1 | 0.93 | 1.68 | 0.2743(2) | 0.2743(3) | (fixed) | 0.00353(14) |
| | 2 | 0.21 | 0.94 | 0.2748(7) | | | |

TABLE 4.3: Pion results for $\beta = 4.0$, fermion mass $m_0 = -0.03$ and $N = \{28, \ldots, 52\}$

### 4.2.3 Results for the Static $Q\bar{Q}$ Potential

In the case of the static $q\bar{q}$ potential, determining the hadron mass at unfixed topology is done exactly in the same way as the pion mass. The static $q\bar{q}$ potential will be considered at the quark separations of $r = \{1a, \ldots, 4a\}$ which gives four different energy levels that can be interpreted as hadron masses. The results for all separations $r$ are summarized in one table for each set of parameters. In order to determine $M(0)$ and $\chi_t$ the strategies c) and d) are applied for all fits. In summary, it can be said that qualitatively similar results are obtained as for the pion mass.

It is noticeable that in particular for $\beta = 3.0$ at separations of $r = 3a, 4a$ the statistical precision of the results is quite low. In particular for $r = 4a$ it can be observed that $M(0)$ obtained by applying c) with $x_Q^{\max} = 5.38$ is closer to the reference value and has a lower statistical error compared to d) with $x_Q^{\max} = 0.73$. This contradicts the fact that the method becomes less precise for larger values of $x_Q$. The reason for this behavior might be found in the fitting of the effective mass plateaus of the static $q\bar{q}$ potential. From figures 4.7 and 4.6 it can be seen that determining the masses $\mathcal{V}_{q\bar{q},Q,V}(3a)$ and $\mathcal{V}_{q\bar{q},Q,V}(4a)$ was problematic due to large statistical errors. Larger statistics would likely solve this problem. For further discussion on this issue see section 4.3. It seems like the value $\chi^2$/dof is a bit more problematic in the case of the static $q\bar{q}$ potential compared to the case of the pion mass. The reason for this remains unclear but it is very likely that it stems from systematic errors which occur during the aforementioned determination of the masses $\mathcal{V}_{q\bar{q},Q,V}(r)$.

| strategy | $r$ | $\chi^2$/dof | $x_Q^{\max}$ | $M(0)$ | $M^{\text{conv}}$ | $\chi_t^{\text{fit}}$ | $\chi_t^{\text{tcd}}$ |
|---|---|---|---|---|---|---|---|
| c) | $a$ | 4.97 | 2.84 | 0.17102(8) | 0.17083(5) | 0.00424(34) | 0.00454(6) |
| d) | $a$ | 1.11 | 0.73 | 0.1713(3) | | (fixed) | |
| c) | $2a$ | 0.32 | 1.30 | 0.2927(19) | 0.2931(3) | 0.00301(305) | 0.00454(6) |
| d) | $2a$ | 0.52 | 0.73 | 0.2923(13) | | (fixed) | |
| (c) | $3a$ | 1.73 | 3.44 | 0.3742(67) | 0.3741(7) | 0.00199(54) | 0.00454(6) |
| | $3a$ | 0.63 | 2.39 | 0.3759(17) | | 0.00354(35) | |
| (d) | $3a$ | 0.25 | 0.73 | 0.3757(36) | | (fixed) | |
| (c) | $4a$ | 1.62 | 5.38 | 0.4263(10) | 0.4272(18) | 0.00252(52) | 0.00454(6) |
| (d) | $4a$ | 0.11 | 0.73 | 0.4295(46) | | (fixed) | |

TABLE 4.4: Static $q\bar{q}$ potential results for $r = \{1a, \ldots, 4a\}$, $\beta = 3.0$, fermion mass $m_0 = -0.07$ and $N = \{28, \ldots, 52\}$

In the case of $\beta = 4.0$ (see table 4.5) it can be observed consistently for all separations $r$ that setting the value of $\chi_t$ to the one of $\chi_t^{\text{tcd}}$ and fixing it yields more precise results compared to using the fitted $\chi_t$. For a separation of $r = a$ and approach d) the extrapolation is shown in figure 4.5.

| strategy | $r$ | $\chi^2$/dof | $x_Q^{\max}$ | $M(0)$ | $M^{\text{conv}}$ | $\chi_t^{\text{fit}}$ | $\chi_t^{\text{tcd}}$ |
|---|---|---|---|---|---|---|---|
| (c) | $a$ | 4.27 | 2.62 | 0.12545(8) | 0.12551(4) | 0.00351(45) | 0.00353(14) |
| (d) | $a$ | 2.07 | 1.11 | 0.12551(9) | | (fixed) | |
| (c) | $2a$ | 5.39 | 3.07 | 0.2246(3) | 0.2247(2) | 0.00349(27) | 0.00353(14) |
| (d) | $2a$ | 5.16 | 3.07 | 0.2246(1) | | (fixed) | |
| (c) | $3a$ | 1.69 | 2.62 | 0.3003(12) | 0.3008(4) | 0.00497(191) | 0.00353(14) |
| (d) | $3a$ | 1.53 | 2.62 | 0.3002(5) | | (fixed) | |
| (c) | $4a$ | 1.98 | 2.62 | 0.3566(26) | 0.3577(9) | 0.00713(774) | 0.00353(14) |
| (d) | $4a$ | 0.47 | 0.94 | 0.3576(2) | | (fixed) | |

TABLE 4.5: Static $q\bar{q}$ potential results for $r = \{1a, \ldots, 4a\}$, $\beta = 4.0$, fermion mass $m_0 = -0.03$ and $N = \{28, \ldots, 52\}$

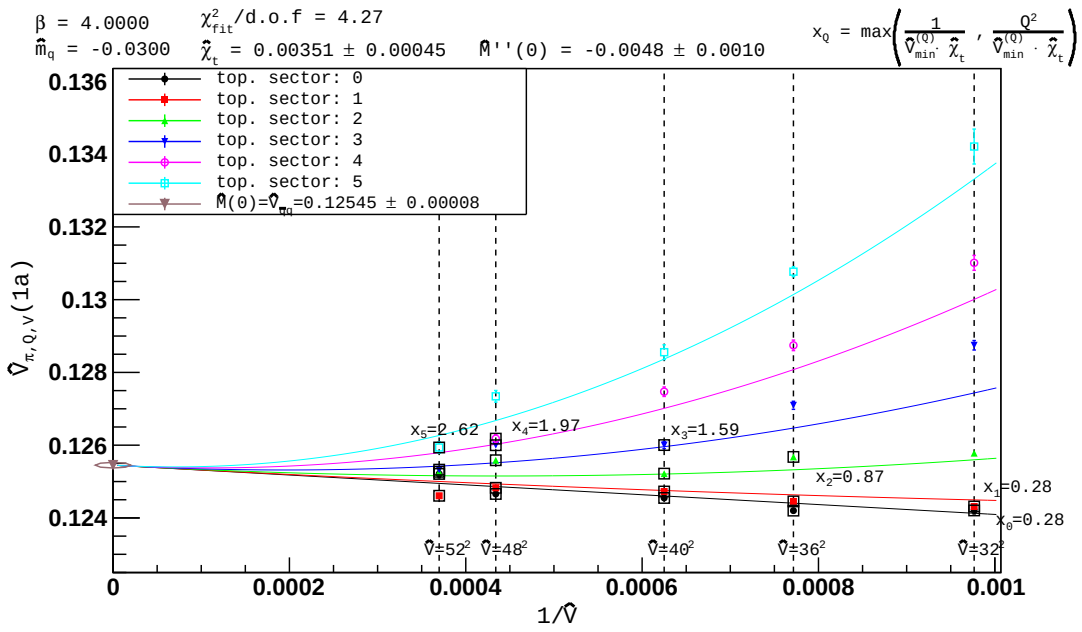


FIGURE 4.5: Hadron mass extrapolation for $\beta = 4.0$, $m_0 = -0.03$, $V = \{32^2, \ldots, 52^2\}$. Reference value of the hadron mass $M^{\text{conv}} = 0.12551(4)$ and of the topological susceptibility $\chi_t = 0.00353(14)$

### 4.2.4 Simultaneous Fitting

As already mentioned in the previous section the idea of simultaneous fitting is to reduce the statistical errors by taking into account a larger amount of data points corresponding to different observables and a single set of parameters. This can be done by creating a combined data set consisting of masses $M_{h_1,Q,V}, \ldots, M_{h_N,Q,V}$ with $h_i$ denoting a specify hadron. With $M_{h_i,Q,V} \equiv M_{i,Q,V}$ one obtains

$$M_{i,Q,V} \approx M_i(0) + \frac{1}{2} M_i''(0) \frac{1}{V \chi_t} \left(1 - \frac{Q^2}{V \chi_t}\right) . \tag{4.6}$$

$\chi_t$ is a common parameter which is simultaneously fitted among all data sets. Hence for $N$ hadrons the total number of parameters to be fitted is given by $P = 2N + 1$. In the case of the pion and the static $q\bar{q}$ potential with quark separations $r = \{1a, \ldots, 4a\}$ the masses $M_{h_i,Q,V}$ of five different hadrons can be combined in a single fit which yields $P = 2 \cdot 5 + 1 = 11$ fit parameters. The combined data sets were created from the selection of $M_{Q,V}$ for $M_{\pi,Q,V}$, $\mathcal{V}_{q\bar{q},Q,V}(r)$ with $(r = \{1a, \ldots, 4a\})$ which have produced the fit results considered the most precise, meaning a value of $M(0)$ which is close to the reference value and a small statistical error.

#### 4.2.4.1 $\beta = 3.0$, fermion mass $m_0 = -0.07$ and $N = \{28, \ldots, 52\}$

In the case of $\beta = 3.0$ (see table 4.6) except for the separation $r = 4a$ of the static $q\bar{q}$ potential the mass $M(0)$ for each observable is more consistent to the corresponding reference value than compared to the single fits. The result for $\chi_t$ deviates by $2.3\sigma$ from the reference value with a statistical error of about 11% which is still not very precise. As it has been shown in the previous section the masses $\mathcal{V}_{q\bar{q},Q,V}(3a)$ and $\mathcal{V}_{q\bar{q},Q,V}(4a)$ are quite problematic because of the large errors on their effective mass curves.

Removing the problematic data and only keeping the data for $M_{\pi,Q,V}$, $\mathcal{V}_{q\bar{q},Q,V}(a)$ and $\mathcal{V}_{q\bar{q},Q,V}(2a)$ leads to the result shown in table 4.7. A further lowering of the statistical error and a closer value of $M(0)$ to the reference value can be observed. $\chi_t$ is now consistent with the reference value within the error but the size of its statistical error has not changed. Due to the consistency it can be considered a fair agreement with the reference value.

| Mass | $M_\pi$ | $\mathcal{V}_{q\bar{q}}(1a)$ | $\mathcal{V}_{q\bar{q}}(2a)$ | $\mathcal{V}_{q\bar{q}}(3a)$ | $\mathcal{V}_{q\bar{q}}(4a)$ |
|---|---|---|---|---|---|
| $M(0)^{\text{prev}}$ | 0.2665(9) | 0.17102(8) | 0.2927(19) | 0.3759(17) | 0.4263(10) |
| $\chi_t^{\text{prev}}$ | 0.00390(155) | 0.00424(35) | 0.00301(305) | 0.00354(35) | 0.00252(52) |
| $M(0)^{\text{new}}$ | 0.2662(2) | 0.17073(8) | 0.2931(3) | 0.3752(5) | 0.4258(17) |
| $\chi_t^{\text{new}}$ | | | 0.00358(39) | | |
| $M(0)^{\text{ref}}$ | 0.2664(2) | 0.17083(5) | 0.2931(3) | 0.3741(7) | 0.4272(18) |
| $\chi_t^{\text{ref}}$ | | | 0.00454(6) | | |

TABLE 4.6: Simultaneous fit results for five data sets: $M_{\pi,Q,V}$, $\mathcal{V}_{q\bar{q},Q,V}(1a)$, $\mathcal{V}_{q\bar{q},Q,V}(2a)$, $\mathcal{V}_{q\bar{q},Q,V}(3a)$, $\mathcal{V}_{q\bar{q},Q,V}(4a)$, parameters: $\beta = 3$, fermion mass $m_0 = -0.07$ and $N = \{28 \ldots 52\}$.

| Mass | $M_\pi$ | $\mathcal{V}_{q\bar{q}}(1a)$ | $\mathcal{V}_{q\bar{q}}(2a)$ |
|---|---|---|---|
| $M(0)^{\text{prev}}$ | 0.2665(9) | 0.17102(8) | 0.2927(19) |
| $\chi_t^{\text{prev}}$ | 0.00390(155) | 0.00424(35) | 0.00301(305) |
| $M(0)^{\text{new}}$ | 0.2664(2) | 0.17081(9) | 0.2933(3) |
| $\chi_t^{\text{new}}$ | | 0.00411(49) | |
| $M(0)^{\text{ref}}$ | 0.2664(2) | 0.17083(5) | 0.2931(3) |
| $\chi_t^{\text{ref}}$ | | 0.00454(6) | |

TABLE 4.7: Simultaneous fit results for three data sets: $M_\pi$,$\mathcal{V}_{q\bar{q},Q,V}(1a)$, $\mathcal{V}_{q\bar{q},Q,V}(2a)$, parameters: $\beta = 3$, fermion mass $m_0 = -0.07$ and $N = \{28 \ldots 52\}$.

#### 4.2.4.2 $\beta = 4.0$, fermion mass $m_0 = -0.03$ and $N = \{28, \ldots, 52\}$

For $\beta = 4.0$ already the single fit results in the previous section 4.2.3 were quite precise. When doing a simultaneous fit this precision can even be improved (see table 4.8). The value for $\chi_t$ is in agreement with the reference value while the uncertainty on $\chi_t$ with approximately 4% is much smaller compared to the case of $\beta = 3.0$. Removing the larger separations of $\mathcal{V}_{q\bar{q}}$ with $r = 3a, 4a$ the changes in the results are of order $10^{-5} - 10^{-6}$ which cannot be seen anymore on the listed values. This suggests that either the determination of the masses $M_{Q,V} = \mathcal{V}_{q\bar{q},Q,V}(3a)$ and $M_{Q,V} = \mathcal{V}_{q\bar{q},Q,V}(4a)$ from the mass curves was already quite precise or that the statistical errors too large and hardly change the fit results. Also the value of $\chi_t$ merely changes.

| Mass | $M_\pi$ | $\mathcal{V}_{q\bar{q}}(1a)$ | $\mathcal{V}_{q\bar{q}}(2a)$ | $\mathcal{V}_{q\bar{q}}(3a)$ | $\mathcal{V}_{q\bar{q}}(4a)$ |
|---|---|---|---|---|---|
| $M(0)^{\text{old}}$ | 0.2749(10) | 0.12545(8) | 0.2246(3) | 0.3003(12) | 0.3566(26) |
| $\chi_t^{\text{old}}$ | 0.00403(133) | 0.00352(45) | 0.00349(27) | 0.00497(191) | 0.00713(714) |
| $M(0)^{\text{new}}$ | 0.2747(2) | 0.12551(4) | 0.2247(2) | 0.3005(3) | 0.3581(7) |
| $\chi_t^{\text{new}}$ | | | 0.00340(14) | | |
| $M(0)^{\text{ref}}$ | 0.2743(3) | 0.12551(4) | 0.2247(2) | 0.3008(4) | 0.3577(9) |
| $\chi_t^{\text{ref}}$ | | | 0.00353(14) | | |

TABLE 4.8: Simultaneous fit results for five data sets: $M_{\pi,Q,V}$, $\mathcal{V}_{q\bar{q},Q,V}(1a)$, $\mathcal{V}_{q\bar{q},Q,V}(2a)$, $\mathcal{V}_{q\bar{q},Q,V}(3a)$, $\mathcal{V}_{q\bar{q},Q,V}(4a)$, parameters: $\beta = 4$, fermion mass $m = -0.03$ and $N = \{28 \ldots 52\}$.

| Mass | $M_\pi$ | $\mathcal{V}_{q\bar{q}}(1a)$ | $\mathcal{V}_{q\bar{q}}(2a)$ |
|---|---|---|---|
| $M(0)^{\text{prev}}$ | 0.2749(10) | 0.12545(8) | 0.2246(3) |
| $\chi_t^{\text{prev}}$ | 0.00403(133) | 0.00352(45) | 0.00349(27) |
| $M(0)^{\text{new}}$ | 0.2747(2) | 0.12551(4) | 0.2247(2) |
| $\chi_t^{\text{new}}$ | | 0.00341(15) | |
| $M(0)^{\text{ref}}$ | 0.2743(3) | 0.12551(4) | 0.2247(2) |
| $\chi_t^{\text{ref}}$ | | 0.00353(14) | |

TABLE 4.9: Simultaneous fit results for three data sets: $M_\pi$,$\mathcal{V}_{q\bar{q}}(1a)$, $\mathcal{V}_{q\bar{q}}(2a)$, parameters: $\beta = 4$, fermion mass $m = -0.03$ and $N = \{28 \ldots 52\}$.

## 4.3 Discussion of Error Sources

In this section the errors are discussed which are considered to affect the results of the infinite volume extrapolations listed in sections 4.2.2 to 4.2.4. The following errors could be identified:

1. Statistical errors (on the effective mass curves):
   The masses $M_{Q,V}$ are obtained by fitting a constant to an effective mass curve which can have large statistical errors, in particular for large temporal separations $n_t$ (c.f. figures 4.6 to 4.9).

2. Systematic errors:

   2.1. Choice of a fitting range for the effective mass plateau:
   This is assumed to be the most influential source of errors. As it can be seen in figures 4.6 to 4.9 it can be quite unclear at which range the effective mass plateaus should be fitted. The choice of the fitting range can easily affect the value of $M_{Q,V}$ up to the order of $10^{-4}$ and in some cases of mass plateaus with a larger statistical error even up to the order of $10^{-3}$. This order is already very relevant for the infinite volume extrapolations since the precision of the results in sections 4.2.2 to 4.2.4 is considered up to the order $10^{-4}$ (for the pion mass) and also in some cases up to $10^{-5}$ (for the static potential). However the statistical errors of $M_{Q,V}$ are of the same order which implies an evening out of the errors allowing for a proper fit.

   2.2. Topology effects (on the effective mass curves):
   It should be mentioned that the topological charge might influence the behavior of the effective mass curves, too. This has already been shown for a quantum mechanical model in [9]. It was observed that the effective mass curves deviate from a plateau at fixed topology. This effect cannot be seen for the mass curves considered in this work. E.g. figure 4.10 shows an effective mass curve at fixed topology with $Q = 2$. No particular behavior can be observed. Just for $n_{t_{\max}}$ the curve increases but this could also be explained by the statistical error. Further mass curves from different simulations have been examined with respect to effects described in [9] for volumes $V = 28^2, \ldots, 52^2$ but no such behavior could be found. The reason could be that either effects are small and larger statistics are needed or that the mass curves have a qualitative different behavior in the Schwinger model.

2.3. Ordinary finite size effects
(occurs for lattices of $V < 44^2$ for the considered parameters $\beta = 3.0$ and $\beta = 4.0$):
Besides statistical and systematic errors ordinary finite size effects should not be neglected. The pion mass is determined by using the operator given by eq.(4.1). For this operator the finite size effects on the mass $M_{Q,V}$ for a space-time volume of $V = 28^2$ is restricted to 0.4% and decrease rapidly, vanishing completely for $V = 44^2$. A finite size effect of 0.4% influences the mass up to the order $10^{-3}$. As explained above, this order is already relevant for the considered precision. The errors stemming from finite size effects can be evened out by statistical errors. However, after restricting $x_Q$ only few points at larger volumes $V \leq 28^2$ are kept in and serve to stabilize the fit.

2.4. Values of $x_Q$:
Another issue is the choice of the values of $x_Q$, in particular the upper limit. It seems like this cannot be defined clearly which might be linked to the errors on $M_{Q,V}$. For the different approaches a)-d) given in section 4.2.1 the largest values of $x_Q$ are different. Hence $x_Q$ can rather be considered an estimate for the precision of the method. In order to make clear statements about $x_Q$ larger statistics would be needed.

One more remark should be made on statistical and systematic errors which seem to be closely linked in the following way. As it can be seen from figures 4.6 to 4.9, the larger the statistical errors are on the effective mass curves the more difficult it becomes to determine a proper fitting range. This makes the process of fitting a constant to an effective mass curve much more prone to systematic errors. Having discussed these points one can consider the errors on the results presented in table 4.4 which seem to be quite large for separations of $r = 3a, 4a$. Especially for time separations $n_t > 10$ (c.f. figure 4.6) the statistical errors become quite large, making it difficult to clearly identify a plateau. For this reason it is likely that the masses $\mathcal{V}_{q\bar{q},Q,V}$ determined by fitting such plateaus are not very reliable. As it can be seen from table 4.5 the problem is less distinct for $\beta = 4.0$, for which the errors start to become large at approximately $n_t > 13$ (c.f. figure 4.7). This can be understood by considering the different size of the lattice spacing for $\beta = 3.0$ which is larger by the factor $\sqrt{4/3} \approx 1.15$. For both values of $\beta$ the same volumes were used ($V = 20^2, \ldots, 52^2$) for the computations which leads to a larger physical volume for the case of $\beta = 3.0$. This explains why the statistical errors for the case of $\beta = 3.0$ are larger at smaller $n_t$ compared to the case for $\beta = 4.0$.

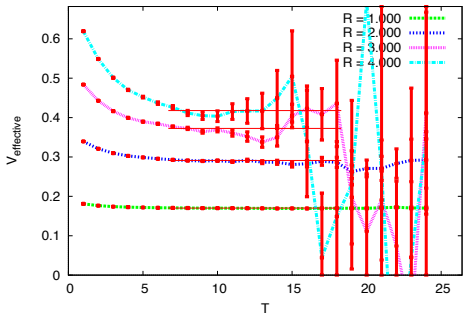


FIGURE 4.6:
Effective mass plateau for $M_{q\bar{q}}^{\text{conv}}$
$\beta = 3.0$, $m_0 = -0.07$, $N_L = 52$.

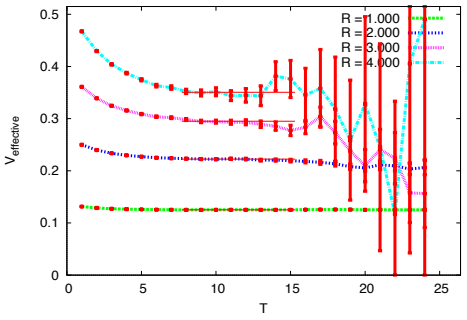


FIGURE 4.7:
Effective mass plateau for $M_{q\bar{q}}^{\text{conv}}$
$\beta = 4.0$, $m_0 = -0.03$, $N_L = 52$.

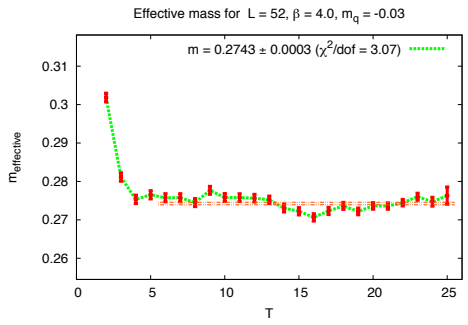


FIGURE 4.8:
Effective mass plateau for $M_{\pi}^{\text{conv}}$,
$\beta = 4.0$, $m_0 = -0.03$, $N_L = 52$.

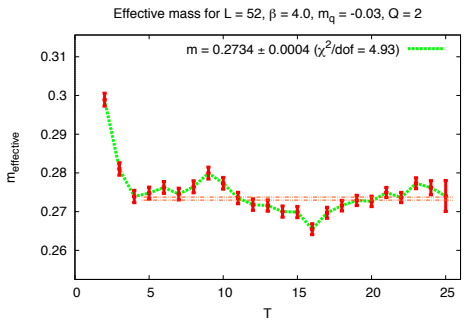


FIGURE 4.9:
Effective mass plateau for $M_{\pi,Q=2,V}$,
$\beta = 4.0$, $m_0 = -0.03$, $N_L = 52$

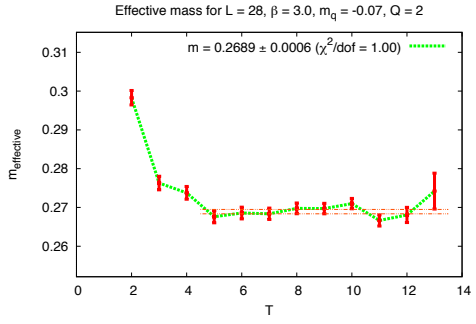


FIGURE 4.10:
Effective mass plateau for $M_{\pi,Q=2,V}$
$\beta = 3.0$, $m_0 = -0.07$, $V = 28^2$.

# Chapter 5

# Conclusions and Outlook

In this work the pion mass and the static potential in the Schwinger model have been successfully determined from computations at fixed topology using a method proposed and equations derived in [6]. The generalization of the method to QCD seems to be straightforward. There it might be used to circumvent problems associated with topology freezing expected at small values of the lattice spacing or when using e.g. overlap fermions.

The method being considered is based on fitting eq.(2.24) to the hadron masses $M_{Q,V}$ at fixed topological sectors and finite volumes. Then the hadron mass in the infinite volume limit (which corresponds to the hadron mass at unfixed topology) is given by the fit parameter $M(0)$ at $\theta = 0$. Eq.(2.24) is an expansion in the parameters $M''(0)\, t/V\, \chi_t\,,\ 1/V\, \chi_t$ and $Q^2/V\, \chi_t$, which must be sufficiently small in order to ensure the validity of this method, though it is difficult to define what exactly "sufficiently small" means. The parameters $1/V\, \chi_t$ and $Q^2/V\, \chi_t$ were referred to as $x_Q$ throughout the results section. For a quantum mechanical model investigated in [9] it was found that $x_Q$ should be $< 0.5$.

However a complete correspondence between the models concerning the values of the expansion parameters can not be assumed. Moreover it turned out that the restriction of $x_Q$ depends on the particular selection of the masses $M_{Q,V}$ to be fitted which seems to be quite arbitrary. For this reason four different ways (c.f. 4.2.1: a-d ) for the systematic selection of the masses $M_{Q,V}$ have been considered. For two of these strategies $x_Q$ had to be restricted to values $< 1$ whereas for the the remaining two strategies $x_Q$ could be unexpectedly large $\lesssim 2.5$. It is likely that this discrepancy is linked to statistical and systematic errors (see section 4.3). More precise data are necessary to study this problem in detail.

Altogether it was observed during the investigations that the method works quite well in particular for the determination of hadron masses, whereas the method is not well suited for determining the topological susceptibility $\chi_t$ precisely. For the presented strategy d) in some cases the fitted $\chi_t$ was consistent with the reference value but had an average error of $\approx 60\%$ leaving the value unusable. Therefore in section 4.2.4 $\chi_t$ was tried to be determined from a simultaneous fit taking into account several sets of data belonging to different observables. This approach proved to yield very good results for the hadron masses as well as quite good results for $\chi_t$. The approach seems to be very promising and attractive for future investigations.

In order to achieve further improvements for this method, eq.(2.24) must be expanded to higher orders. Another way which might lead to improvements is directly fitting the correlation function using an exponential model containing eq.(2.24) and higher orders of it. The idea is to obtain a more systematic approach for choosing the fitting range and being able to directly obtain the hadron mass $M(0)$ at unfixed topology, instead of determining $M_{Q,V}$ from effective mass plateaus (which is highly prone to human errors) and trying to obtain $M(0)$ from fitting eq.(2.24) to the masses $M_{Q,V}$. This work is in progress.

# Appendix A

# Theoretical Appendix

## A.1 Derivation of the Topological Charge in 1+1-Dimensions

Consider gauge fields with a finite action which gauge equivalent to $A_\mu = 0$ on the border of the 1+1 dimensional space-time. A gauge transformation

$$A_\mu \to A'_\mu = gA_\mu g^{-1} - \frac{i}{e}(\partial_\mu g)g^{-1}, \quad g \in U(1) \tag{A.1}$$

yields, for gauge fields on the border of the 1+1 dimensional space-time with $A_\mu = 0$ :

$$A'_\mu = -i\frac{1}{e}(\partial_\mu g)g^{-1}. \tag{A.2}$$

Inserting the parametrization $g(\phi) = \exp(i\Lambda(\phi))$ with $\Lambda(\phi) \in \mathbb{R}$ leads to

$$A'_\mu = \frac{1}{e}\,\partial_\mu \Lambda(\phi)\ , \qquad \Rightarrow \qquad e\,A'_\mu = \partial_\mu \Lambda(\phi)\ . \tag{A.3}$$

Consider $g(\phi)$, which is $2\pi-$periodic: $g(\phi + 2\pi) = g(\phi)$, accordingly

$$g(\Lambda(\phi + 2\pi)) = g(\Lambda(\phi) + 2\pi n) \tag{A.4}$$

$$\Rightarrow \Lambda(\phi + 2\pi) = \Lambda(\phi) + 2\pi n \tag{A.5}$$

$$\Rightarrow \Lambda(\phi + 2\pi) - \Lambda(\phi) = 2\pi n \tag{A.6}$$

Since $\partial_\phi \Lambda$ is $2\pi$-periodic the left hand side of eq.(A.6) can be rewritten into

$$\int_0^{2\pi} \frac{\partial \Lambda}{\partial \phi} \mathrm{d}\phi = 2\pi n \quad \Rightarrow \quad \frac{1}{2\pi} \int_0^{2\pi} \partial_\phi \Lambda \, \mathrm{d}\phi = n \; . \tag{A.7}$$

The partial derivative $\partial_\phi \Lambda$ can be reformulated into

$$\partial_\phi \Lambda = \partial_\phi x^\mu \, \partial_\mu \Lambda \; . \tag{A.8}$$

Inserting this expression into eq.(A.7) yields

$$\frac{1}{2\pi} \int_0^{2\pi} \partial_\phi x^\mu \, \partial_\mu \Lambda \, \mathrm{d}\phi = n \quad \Rightarrow \frac{1}{2\pi} \int_0^{2\pi} \underbrace{\partial_\phi x^\mu \, d\phi}_{=\mathrm{d}x^\mu} \, \partial_\mu \Lambda = n \tag{A.9}$$

In this expression $\partial_\mu \Lambda$ can be replaced by the left hand side of eq.(A.3) in order to obtain

$$\frac{e}{2\pi} \int_0^{2\pi} \mathrm{d}x^\mu \, A_\mu = n \; . \tag{A.10}$$

This expression can be considered a line integral over the border of the $1+1$-dimensional space-time. Finally Stoke's theorem can be applied:

$$\begin{aligned} n &= \frac{e}{2\pi} \oint_{\partial S} d\vec{s} \cdot \vec{A} && \text{(A.11)} \\ &= \frac{e}{2\pi} \int_S d\vec{S} \left( \vec{\nabla} \times \vec{A} \right) && \text{(A.12)} \\ &= \frac{e}{2\pi} \int_S d^2x (\partial_x A_y - \partial_y A_x) && \text{(A.13)} \\ &= \frac{e}{2\pi} \int_S d^2x F_{12}, && \text{(A.14)} \end{aligned}$$

with $n$ defining the topological charge $n := Q$.

## A.2 The $Q-$Dependent Hadron Mass

This section contains a detailed derivation of Eq.(2.24). Principally it is based on what has been done in a concise form in [6, 8]. The main part of the derivation, which will take place in section A.2.2, deals with finding an expression for the topological charge and space-time volume dependent correlation function $C_{Q,V}$ which allows for an appropriate expansion in its exponential form. The starting point for the derivation is considering the partition function $Z_{Q,V}$ at fixed topological charge $Q$.

### A.2.1 The Partition Function

Assuming the fermion fields are integrated out an effective gauge action $S_{\text{eff}}[U]$ remains in the partition function which contains the fermion determinant. The partition function then reads:

$$Z = \int \mathrm{D}U \, e^{S_{\text{eff}}[U]}. \tag{A.15}$$

This form will be kept throughout the calculation for convenience. In order to separate gauge configurations analytically from different topological sectors a Kronecker delta is inserted into the partition function for filtering gauge configurations which do not belong to a certain topological sector:

$$\delta_{Q,Q[U]} = \frac{1}{2\pi} \int_{-\pi}^{\pi} \mathrm{d}\theta \, e^{i\theta(Q-Q[U])}. \tag{A.16}$$

The partition function then becomes topological charge dependent. Inserting the Kronecker delta and rearranging the terms in the following manner gives rise to the $\theta-$dependent partition function.

$$Z_Q = \overbrace{\int \mathrm{D}U \, e^{S_{\text{eff}}[U]}}^{Z} \overbrace{\frac{1}{2\pi} \int_{-\pi}^{\pi} \mathrm{d}\theta \, e^{i\theta(Q-Q[U]}}^{\delta_{Q,Q[U]}} \tag{A.17}$$

$$= \frac{1}{2\pi} \int_{-\pi}^{\pi} \mathrm{d}\theta \, e^{i\theta Q} \underbrace{\int \mathrm{D}[U] \, e^{-S_{\text{eff}}[U]-i\theta Q[U]}}_{Z(\theta),} \tag{A.18}$$

$$= \frac{1}{2\pi} \int_{-\pi}^{\pi} \mathrm{d}\theta \, e^{i\theta Q} \tag{A.19}$$

Note that in this expression $Z(\theta = 0) = Z$ and $Z(\theta) = Ze^{-i\theta Q[U]}$. Hence the second derivative of $Z(\theta)$ with respect to $\theta$ at $\theta = 0$ equals the expectation value of the squared topological charge:

$$-\frac{\partial Z(\theta)}{\partial \theta^2}\bigg|_{\theta=0} = \langle Q^2 \rangle, \tag{A.20}$$

which is related to the topological susceptibility and the space-time volume by

$$\langle Q^2 \rangle = V \chi_t. \tag{A.21}$$

This leads to the suggestion that $Z(\theta)$ can be expressed as follows:

$$Z(\theta) = \underbrace{\int \mathrm{D}U\, e^{S_{\mathrm{eff}}[U]}}_{Z}\; e^{-\frac{1}{2}V\chi_t\theta^2}, \tag{A.22}$$

$$= \quad Z \quad e^{-\frac{1}{2}V\chi_t\theta^2}. \tag{A.23}$$

Substituting this expression into eq.(A.19) results in

$$Z_Q = \frac{1}{2}\int_{-\pi}^{\pi} \mathrm{d}\theta\, e^{i\theta\nu} \int \mathrm{D}[U]\, e^{-S_{\mathrm{eff}}[U]-\frac{1}{2}V\chi_t\theta^2}. \tag{A.24}$$

Note that now the $V$ dependence of $Z_Q$ becomes obvious and for this reason from now on $Z_Q = Z_{Q,V}$ will be used. Rearranging the terms gives

$$Z_{Q,V} = \frac{1}{2}\int_{-\pi}^{\pi} \mathrm{d}\theta \int \mathrm{D}[U]\, e^{-S_{\mathrm{eff}}[U]}\, e^{i\theta Q-\frac{1}{2}V\chi_t\theta^2} \tag{A.25}$$

$$= \frac{1}{2}\int_{-\pi}^{\pi} \mathrm{d}\theta\, Z\, e^{i\theta Q-\frac{1}{2}V\chi_t\theta^2}. \tag{A.26}$$

This integral can be evaluated by applying a saddle point approximation. Substituting the argument of the exponential by

$$u(\theta) = -\frac{V\chi_t}{2}\theta^2 + iQ\theta, \tag{A.27}$$

a stationary phase of the integral in eq.(A.26) can be found by minimizing $u(\theta)$:

$$\frac{\partial u(\theta)}{\partial\theta} = 0 \to \theta_s = i\frac{Q}{V\chi_t}. \tag{A.28}$$

Reformulating $u(\theta)$ by completing the square yields

$$u(\theta) = -\frac{V\chi_t}{2}\theta^2 + iQ\theta, \tag{A.29}$$

$$= -\frac{Q^2}{2V\chi_t} - \frac{1}{2}\left(\theta-\theta_s\right)^2 V\chi_t, \tag{A.30}$$

Inserting this expression into eq.(A.26) a Gaussian integral is obtained:

$$Z_{Q,V} = \frac{1}{2\pi}\int_{-\pi}^{\pi} \mathrm{d}\theta\, Z\, e^{-\frac{Q^2}{2V\chi_t}}\, e^{-\frac{1}{2}(\theta-\theta_s)^2 V\chi_t}. \tag{A.31}$$

Applying the substitution $s = (\theta-\theta_s)\sqrt{V\chi_t}$ gives

$$Z_{Q,V} = \frac{1}{2\pi\sqrt{V\chi_t}}\int_{s(-\pi)}^{s(\pi)} \mathrm{d}s\, Z\, e^{-\frac{Q^2}{2V\chi_t}}\, e^{-\frac{s^2}{2}}. \tag{A.32}$$

For finite limits of the integral the result can be expressed in terms of two error functions:

$$Z_{Q,V} = -\frac{Z\, e^{-\frac{Q^2}{2V\chi_t}}}{2\pi V\chi_t} \underbrace{\sqrt{\frac{\pi}{2}} \left[ \operatorname{erf}\left( \frac{\theta_s - \pi\sqrt{V\chi_t}}{\sqrt{2}} \right) - \operatorname{erf}\left( \frac{\theta_s + \pi\sqrt{V\chi_t}}{\sqrt{2}} \right) \right]}_{c_{\mathrm{erf}}}. \tag{A.33}$$

For sufficiently large values of $V\chi_t \gg 1$ the value of $c_{\mathrm{erf}}$ is a good approximation for $\sqrt{2\pi}$. Using the fact that $\theta_s = iQ/V\chi_t$, a further property which is favorable for this approximation, is a small absolute value of the topological charge $|Q|$. This should be noted as the central point of this derivation.

### A.2.2 Correlation Functions at Fixed Topological Sectors

The starting point shall be the $Q$ and $V$ dependent correlation function, cf. eq.(2.21)

$$C_{Q,V} = \frac{1}{Z_{Q,V}} \frac{1}{2\pi} \int_{-\pi}^{\pi} \mathrm{d}\theta\, Z(\theta)\, C(\theta)\, e^{i\theta Q}, \tag{A.34}$$

Reformulating eq.(A.34) completely analogous to (A.19 - A.33) one arrives at

$$C_{Q,V} = \frac{Z\, e^{-\frac{Q^2}{2V\chi_t}}}{Z_{Q,V}\, 2\pi\sqrt{V\chi_t}} \int_{s(-\pi)}^{s(\pi)} \mathrm{d}s\, C\left( \theta_s + \frac{s}{\sqrt{V\chi_t}} \right) e^{-\frac{s^2}{2}}. \tag{A.35}$$

At this point it is possible to almost fully cancel the factor in front of the integral by inserting $Z_{Q,V}$ from eq.(A.33) and assuming $c_{\mathrm{erf}} = 2\pi$ (c.f. eq.(A.33)). The correlation function reduces to

$$C_{Q,V} = \frac{1}{\sqrt{2\pi}} \int_{s(-\pi)}^{s(\pi)} \mathrm{d}s\, C\left( \theta_s + \frac{s}{\sqrt{V\chi_t}} \right) e^{-\frac{s^2}{2}}. \tag{A.36}$$

In order to evaluate the integral a development around $s = 0$ is done:

$$C\left( \theta_s + \frac{s}{\sqrt{V\chi_t}} \right) = C(\theta_s) + \frac{C'(\theta_s)}{\sqrt{V\chi_t}}\, s + \frac{C''(\theta_s)}{2V\chi_t}\, s^2 + \mathcal{O}(s^3). \tag{A.37}$$

Because of the symmetry $C(\theta) = C(-\theta)$ the odd orders of the derivative of $C(\theta_s)$ vanish. The assumption of $V\chi_t \gg 1$ leads to

$$C\left( \theta_s + \frac{s}{\sqrt{V\chi_t}} \right) \approx C(\theta_s) + \frac{C''(\theta_s)}{2V\chi_t}\, s^2. \tag{A.38}$$

Inserting this approximation into eq.(A.35) gives

$$C_{Q,V} = \frac{1}{\sqrt{2\pi}} \left[ \int_{s(-\pi)}^{s(\pi)} \mathrm{d}s\, C(\theta_s)\, e^{-\frac{s^2}{2}} + \int_{s(-\pi)}^{s(\pi)} \mathrm{d}s\, \frac{C''(\theta_s)}{2V\chi_t}\, s^2\, e^{-\frac{s^2}{2}} \right] \tag{A.39}$$

$$= \frac{1}{\sqrt{2\pi}} \left[ \sqrt{2\pi}\, C(\theta_s) + \sqrt{2\pi}\, \frac{C''(\theta_s)}{2V\chi_t} \right] \tag{A.40}$$

$$= C(\theta_s) + \frac{1}{2V\chi_t}\, C''(\theta_s), \tag{A.41}$$

At this point a crucial simplification is carried out. Once again the saddle point $\theta_s = i\nu/V\chi_t$ is used as in section A.2.1. This is only a good approximation if the condition is fulfilled that the value of $M''(0)t/V\chi_t$ is sufficiently small. Searching for the correct saddle point for the right side of eq.(A.36) would lead to a rather lengthy calculation but under certain approximations the same result would be obtained as in the following section A.2.3. For reasons of simplicity the rather lengthy derivation is left out here.

### A.2.3 The Particle Mass at Fixed Topological Sectors

In order to find an expression for the particle mass the next step is to insert expressions for $C(\theta_s)$ and $C''(\theta_s)$ into eq.(A.41). The expression for the correlation function can be derived by following the description given in A.3. In the following the $\theta$-dependent correlation function is considered at the saddle point $\theta_s = i\,Q/(V\chi_t)$, hence

$$C(\theta_s) = \underbrace{|\langle 0, \theta_s | O | 1, \theta_s \rangle|^2}\, e^{-M(\theta_s)\,(t)} \tag{A.42}$$

$$= \qquad A(\theta) \qquad e^{-M(\theta_s)\,(t)}. \tag{A.43}$$

In this expression $M(\theta_s)$ can be expanded:

$$M(\theta_s) = M(0) + \frac{1}{2} M''(0)\, \theta_s^2 + \mathcal{O}\left(\theta_s^4\right). \tag{A.44}$$

Using this expansion and computing the second derivative of $C(\theta_s)$ the insertion into eq.(A.41) leads to

$$C_{Q,V} = \left( A(\theta_s) + \frac{A''(\theta_s)}{2V\chi_t} - \frac{A(\theta_s)\, M''(0)\, t}{2V\chi_t} \right) e^{-\left(M(0) + \frac{1}{2}M''(0)\,\theta_s^2 + \mathcal{O}\left(\theta_s^4\right)\right) t} \tag{A.45}$$

$$- \left( \frac{A^2(\theta) M''(0)}{V\chi_t}\, \theta\, t + \frac{A(\theta)(M''(0))^2}{2V\chi_t}\, \theta^2 t^2 \right) e^{\left(M(0) + \frac{1}{2}M''(0)\,\theta_s^2 + \mathcal{O}\left(\theta_s^4\right)\right) t},$$

where the second term on the right hand side is put into an error term:

$$C_{Q,V} = \left( A(\theta_s) + \frac{A''(\theta_s)}{2V\chi_t} - \frac{A(\theta_s)\, M''(0)\, t}{2V\chi_t} \right) e^{-\left(M(0)+\frac{1}{2}M''(0)\,\theta_s^2+\mathcal{O}\left(\theta_s^4\right)\right)t} \tag{A.46}$$

$$+ \mathcal{O}\left(\frac{1}{V^2}\right). \tag{A.47}$$

A rearrangement of the terms leads to

$$C_{Q,V} = A(\theta_s) \left( 1 + \frac{A''(\theta_s)}{2A(\theta_s)V\chi_t} - \frac{M''(0)\, t}{2V\chi_t} \right) e^{-\left(M(0)+\frac{1}{2}M''(0)\,\theta_s^2+\mathcal{O}\left(\theta_s^4\right)\right)t} \tag{A.48}$$

$$+ \mathcal{O}\left(\frac{1}{V^2}\right). \tag{A.49}$$

Approximating the expression in the parenthesis as an exponential yields

$$C_{Q,V} = A(\theta)\, e^{\frac{A''(\theta_s)}{2A(\theta)V\chi_t} - \frac{M''(0)\,t}{2V\chi_t}} e^{-\left(M(0)+\frac{1}{2}M''(0)\,\theta_s^2+\mathcal{O}\left(\theta_s^4\right)\right)t} + \mathcal{O}\left(\frac{1}{V^2}\right). \tag{A.50}$$

A further rearrangement and the use of $\theta_s^2 = (iQ/(V\chi_t))^2$ then gives

$$C_{Q,V} = \underbrace{A(\theta)\, e^{\frac{A''(\theta_s)}{2A(\theta)V\chi_t}}}\ \underbrace{e^{-\left(\frac{M''(0)}{2V\chi_t}+M(0)+\frac{M''(0)}{2V\chi_t}Q^2+\mathcal{O}\left(\theta_s^4\right)\right)t}} + \mathcal{O}\left(\frac{1}{V^2}\right). \tag{A.51}$$

$$= \qquad A_Q \qquad\qquad\qquad e^{-M_Q\, t} \qquad + \mathcal{O}\left(\frac{1}{V^2}\right). \tag{A.52}$$

which finally leads to

$$M_Q = M(0) + \frac{1}{2}\, M''(0)\, \frac{1}{V\chi_t} \left( 1 - \frac{Q^2}{V\chi_t} \right) + \mathcal{O}\left(\frac{1}{V^2}\right). \tag{A.53}$$

which represents the central equation of this work.

Principally higher orders of this expression could be computed but in this case the effective mass $M_\nu$ would become time dependent. The reason for this is given by the property of nonlocality of QCD at fixed topological charge. In this case the theory would not even have a Hamiltonian [6].

## A.3 Extraction of the hadron masses

In order to determine the pion mass the expectation value of a two point correlation function must be evaluated. In general the expectation value of a Euclidean two point correlation function can be expressed in terms of path integrals in the following way:

$$C(t_1 - t_2) = \langle O_1(t_1) O_2(t_2) \rangle \tag{A.54}$$

$$= \int \mathrm{D}[U]\, \mathcal{O}_1(t_1) \mathcal{O}_2(t_2)\, e^{-S_{\mathrm{eff}}[U]}. \tag{A.55}$$

$$= \frac{1}{Z} \sum_m \langle m | e^{-\hat{H}\,(T - t_1 + t_2)}\, O_1\, e^{-\hat{H}\,(t_1 - t_2)}\, O_2 | m \rangle \tag{A.56}$$

$$= \frac{1}{Z} \sum_{m,n} e^{-E_m\,(T - t_1 + t_2)} \langle m | O_2 | n \rangle\, e^{-E_n\,(t_1 - t_2)}\, \langle n | O_1 | m \rangle. \tag{A.57}$$

Where the general pair of operators

$$O_1 = \bar{\psi}_{t_2} \Gamma_1 \psi_{t_2} \quad \text{and} \quad O_2 = \bar{\psi}_{t_1} \Gamma_2 \psi_{t_1} \tag{A.58}$$

creates an up-quark and a down-antiquark at $t_1$ and annihilates them at $t_2$. In the case of two point correlation functions the operators $O_2$ and $O_1$ are the complex conjugates of each other and hence the expression can be written as

$$C(t_1 - t_2) = \frac{1}{Z} \sum_{m,n} |\langle m | O | n \rangle|^2\, e^{-E_m\, T}\, e^{-[\,E_n - E_m\,]\,(t_1 - t_2)}. \tag{A.59}$$

The difference $E_n - E_m$ can be measured experimentally. For sufficiently large temporal volumes $T \gg 1$ only the vacuum state with $E_m = E_0$ survives and for large time separations $(t_1 - t_2)$ the higher energy contributions with $E_n - E_0$ with $n > 1$ become very small. Defining $\Delta E_n = E_n - E_0$ eq.(A.59) becomes

$$C(t_1 - t_2) = \frac{e^{-E_0\, T}}{Z} |\langle 0 | O | 1 \rangle|^2\, e^{-[\,\Delta E_1\,]\,(t_1 - t_2)} \left(1 + \mathcal{O}\left(e^{\Delta E_2\,(t_1 - t_2)}\right)\right). \tag{A.60}$$

The effective particle mass is now given by the ground state Energy of the hadron with $M_{\mathrm{eff}} = \Delta E_1$. The exponential containing the ground state energy is canceled by the factor $\frac{1}{Z}$ due to

$$Z = \int \mathrm{D}[U]\, e^{-S_{\mathrm{eff}}[U]} = \sum_n \langle n|e^{-H\,T}|n\rangle \tag{A.61}$$

$$= \sum_n e^{-E_n\,T} \overset{T\gg 1}{=} e^{-E_0\,T}. \tag{A.62}$$

Substituting $t = t_1 - t_2$ the expression for the meson correlator reads

$$C(t) = A\, e^{-\,\Delta E_1\,(t)} \left(1 + \mathcal{O}\left(e^{\Delta E_2\,(t)}\right)\right), \tag{A.63}$$

where $\Delta E_2$ is the energy difference to the first excited state. By expressing the time $t$ in units of the lattice constant $a$ via $t = n_t\, a$ ($n_t$ denotes the lattice sites in time direction) an effective mass can be defined:

$$M_{\mathrm{eff}}\left(n_t\, a + \frac{1}{2}\, a\right) = \ln\left(\frac{C(n_t\, a)}{C(n_t\, a + a)}\right). \tag{A.64}$$

At this point the lattice spacing $a$ can be dropped and $C(n_t)$ can be considered at the lattice sites $n_t$. As soon as the correlation function $C(n_t)$ is dominated by the ground state $\Delta E_1$ the higher energy contributions from the sub-leading exponentials can be neglected - the effective mass $M_{\mathrm{eff}}$ becomes constant. Due to the periodical boundary conditions of the lattice and the symmetry properties of the correlation function, the exponential function must be replaced by a cosh-function:

$$e^{-\,\Delta E_1\,(n_t)} \longrightarrow \frac{1}{2}\left(e^{-\,\Delta E_1\,(n_t)} + e^{-\,\Delta E_1\,(N_T - n_t)}\right). \tag{A.65}$$

Therefore eq.(A.64) assumes the more complicated form of

$$M_{\mathrm{eff}}\left(n_t + \frac{1}{2}\right) = \ln\left(\frac{C(n_t)}{C(n_t + 1)}\right) = \ln\left(\frac{\cosh(M_{\mathrm{eff}}(n_t - N_T/2))}{\cosh(M_{\mathrm{eff}}(n_t + 1 - N_T/2))}\right). \tag{A.66}$$

In order to extract the effective mass eq.(A.66) has to be solved for $M_{\mathrm{eff}}$ at each time slice. Then a curve is plotted with the values of $M_{\mathrm{eff}}$ for each time slice. Afterwards a constant fit has been done in the region where $M_{\mathrm{eff}}$ has become constant which is considered as the effective mass plateau.

# *Acknowledgements*

Writing this thesis would not have been possible without the kind people who shared time to support me, to only some of whom it is possible to give particular mention here.
First of all I want to thank my supervisor Marc Wagner who guided me and accompanied my work and always shared time for discussion whenever it was needed.
I am extremely grateful for the time my colleague Arthur Dromard spent in order to give me advice on the topic of this work whenever it was necessary.
I want to thank my colleague David Palao for supporting me in technical questions many times.
I want to thank Carsten Urbach for providing the Hybrid Monte Carlo algorithm which all the simulations, performed for this work, are based on. Furthermore I want to thank him for inviting me to the university of Bonn in order to give me advice on how to use the Hybrid Monte Carlo algorithm.
I want to thank Wolfgang Unger, Georg Bergner, Wolfgang Bietenholz, Gregorio Herdoiza and Krzysztof Cichy for discussion.

# Bibliography


[1] M. Lüscher and S. Schaefer, JHEP **1107**, 036 (2011) [arXiv:1105.4749 [hep-lat]].

[2] S. Aoki *et al.* [JLQCD Collaboration], Phys. Rev. D **78**, 014508 (2008) [arXiv:0803.3197 [hep-lat]].

[3] H. Fukaya *et al.*, Phys. Rev. D **73**, 014503 (2006) [hep-lat/0510116].

[4] W. Bietenholz *et al.*, JHEP **0603**, 017 (2006) [hep-lat/0511016].

[5] F. Bruckmann *et al.*, Eur. Phys. J. A **43**, 303 (2010) [arXiv:0905.2849 [hep-lat]].

[6] R. Brower, S. Chandrasekharan, J. W. Negele and U. J. Wiese, Phys. Lett. B **560** (2003) 64 [hep-lat/0302005].

[7] S. Aoki, H. Fukaya, S. Hashimoto and T. Onogi, Phys. Rev. D **76** (2007) 054508 [arXiv:0707.0396 [hep-lat]].

[8] W. Bietenholz and I. Hip, J. Phys. Conf. Ser. **378** (2012) 012041 [arXiv:1201.6335 [hep-lat]].

[9] A. Dromard and M. Wagner, arXiv:1309.2483[hep-lat].

[10] S. R. Coleman, Annals Phys. **101** (1976) 239.

[11] S. R. Coleman, R. Jackiw and L. Susskind, Annals Phys. **93** (1975) 267.

[12] C. Gattringer, Annals Phys. **250** (1996) 389 [hep-th/9602027].

[13] D. Alm, Untersuchung des Hybrid-Mote-Carlo-Algorithmus am Beispiel des 2D-Schwingermodells, Bachelor Thesis, University Bonn (2012)

[14] C. R. Gattringer, I. Hip and C. B. Lang, Nucl. Phys. B **508**, 329 (1997) [hep-lat/9707011].

[15] M. Lüscher, Commun. Math. Phys. **85**, 39 (1982).

[16] A. V. Smilga, Phys. Rev. D **55** (1997) 443 [hep-th/9607154].

[17] C. Gattringer, I. Hip and C. B. Lang, Phys. Lett. B **466** (1999) 287 [hep-lat/9909025].

[18] P. Buividovich, C. Urbach, Tutorial on the Hybrid Monte-Carlo method, Dubna (2011)
`http://www.lattice.itep.ru/ pbaivid/dubna/`

[19] M. Lüscher, Phys. Lett. B **428** (1998) 342 [hep-lat/9802011].

[20] Christian Wiese, Efficient computation of meson and four-quark correlation functions, Master Thesis, Homboldt-Universität zu Berlin, September 2012.

[21] L. Del Debbio, L. Giusti and C. Pica, Phys. Rev. Lett. **94** (2005) 032003 [hep-th/0407052].

[22] R. Peccei, The strong CP Problem, in: CP violation, C. Jarlskog (ed.), World Scientific, Singapore 1989

[23] C. Gutsfeld, H. A. Kastrup and K. Stergios, Nucl. Phys. B **560** (1999) 431 [hep-lat/9904015].

[24] N. Christian, K. Jansen, K. Nagai and B. Pollakowski, Nucl. Phys. B **739** (2006) 60 [hep-lat/0510047].

[25] M. Luscher, Commun. Math. Phys. **104** (1986) 177.

[26] `https://github.com/urbach/schwinger`.